Two-Wave Nanotherapy To Target the Stroma and Optimize Gemcitabine Delivery To a Human Pancreatic Cancer Model in Mice

Huan Meng,[†,*] Yang Zhao,[†] Juyao Dong,[‡] Min Xue,[‡] Yu-Shen Lin,[∥] Zhaoxia Ji,[§] Wilson X. Mai,[†] Haiyuan Zhang,[†] Chong Hyun Chang,[§] C. Jeffrey Brinker,[⊥,¶] Jeffrey I. Zink,[‡,§] and Andre E. Nel[†,§,*]

[†]Division of NanoMedicine, Department of Medicine, [‡]Department of Chemistry & Biochemistry, and [§]California NanoSystems Institute, University of California, Los Angeles, California 90095, United States, [⊥]Self-Assembled Materials Department, Sandia National Laboratories, Albuquerque, New Mexico 87185, United States, [∥]Center for Micro-Engineered Materials, The University of New Mexico, Albuquerque, New Mexico 87131, United States, and [¶]Department of Chemical and Nuclear Engineering, The University of New Mexico, Albuquerque, New Mexico 87131, and Sandia National Laboratories, Albuquerque, New Mexico 87106, United States

ABSTRACT Pancreatic ductal adenocarcinoma (PDAC) elicits a dense stromal response that blocks vascular access because of pericyte coverage of vascular fenestrations. In this way, the PDAC stroma contributes to chemotherapy resistance in addition to causing other problems. In order to improve the delivery of gemcitabine, a first-line chemotherapeutic agent, a PEGylated drug-carrying liposome was developed, using a transmembrane ammonium sulfate gradient to encapsulate the protonated drug up to 20% w/w. However, because the liposome was precluded from entering the xenograft site due to the stromal interference, we developed a first-wave nanocarrier that decreases pericyte coverage of the vasculature through interference in the pericyte recruiting TGF-β signaling pathway. This was accomplished using a polyethyleneimine (PEI)/polyethylene glycol (PEG)-coated mesoporous silica nanoparticle (MSNP) for molecular complexation to a small molecule TGF-β inhibitor, LY364947. LY364947 contains a nitrogen atom that attaches, through H-bonding, to PEI amines with a high rate of efficiency. The copolymer coating also facilitates systemic biodistribution and retention at the tumor site. Because of the high loading capacity and pH-dependent LY364947 release from the MSNPs, we achieved rapid entry of IV-injected liposomes and MSNPs at the PDAC tumor site. This two-wave approach provided effective shrinkage of the tumor xenografts beyond 25 days, compared to the treatment with free drug or gemcitabine-loaded liposomes only. Not only does this approach overcome stromal resistance to drug delivery in PDAC, but it also introduces the concept of using a stepwise engineered approach to address a range of biological impediments that interfere in nanocancer therapy in a spectrum of cancers.

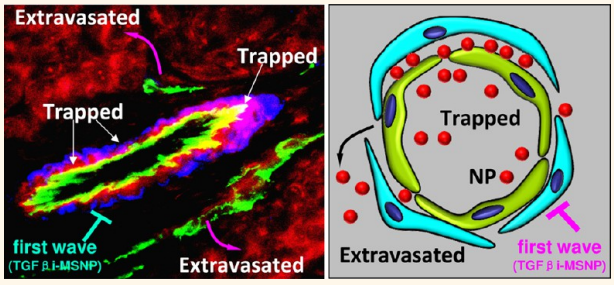

KEYWORDS: nano-engineered approach · two-wave · pancreatic cancer · pericyte and stroma · TGF-β · gemcitabine · mesoporous silica nanoparticles · liposome

Human pancreatic ductal adenocarcinoma (PDAC) is the fourth leading cause of cancer-related death in the United States, with a median survival of <6 months.[1] Since PDAC is typically diagnosed at a late stage, many PDAC cases cannot be considered for surgery because of metastases and spread to the mesenteric circulation and regional lymph nodes at the time of diagnosis.[2,3] Although chemotherapy is often the only treatment option, this approach is characterized by poor efficacy and serious side effects. While most cultured PDAC cells are relatively sensitive to cancer drugs such as gemcitabine (GEM), paclitaxel, and 5-FU, clinical treatment is often unsuccessful because of the dense stromal barrier, which is a histological hallmark of PDAC.[4] The desmoplastic stroma comprises a dense extracellular matrix, as well as a

* Address correspondence to anel@mednet.ucla.edu, hmeng@mednet.ucla.edu.

Received for review August 5, 2013 and accepted October 21, 2013.

Published online October 21, 2013
10.1021/nn404083m

variety of noncancerous cells, including pericytes, which block vascular fenestrations and prevent vascular access of cancer drugs and other therapeutics.[4−8] This includes interference in the delivery of drug-transporting nanocarriers in animal PDAC models.[5−8] Pericyte (PC) coverage of more than 70% of the tumor vasculature significantly differentiates PDAC from other cancer types that exhibit a lesser stroma, such as glioblastoma or renal carcinoma. The percent of pericyte coverage in the latter tumors is only 10−20%,[4−6] with mammary and colon carcinoma occupying an intermediary position.[4−6] Thus, the development of efficacious and safe chemotherapy for PDAC presents a major challenge as a result of the stromal effects.

A number of strategies have been pursued to improve chemotherapy in PDAC patients. These efforts have involved improvement of the pharmacokinetic profile, tumor-specific targeting, and attempts to overcome the resistance of the stromal barrier.[9−12] One promising approach is to take advantage of the ability of nanocarriers to encapsulate and deliver chemotherapeutic agents to improve drug stability and cytotoxic killing. For instance, free GEM, which is a first-line chemotherapeutic agent in PDAC, has a very short half-life *in vivo* (on the order of minutes) and is rapidly degraded by cytidine deaminase (CDA) in the circulation and at the tumor site.[13] Use of a nanocarrier, such as a unilamellar PEGylated liposome, has been shown to increase GEM plasma half-life and intratumoral drug concentration, to the extent that a 10-fold lower drug dose could be used to achieve tumor inhibition in mice, without signs of toxicity.[11] Nanocarriers could, however, also be used to overcome stromal resistance by alteration or elimination of the reactive stromal compartment, which can increase the bioavailability of cancer drugs at the PDAC site.[14] Tumor angiogenesis, blood vessel stability, and vascular access are controlled by a number of important growth factors, including a key contribution by transforming growth factor beta (TGF-β), which promotes pericyte coverage of vascular fenestrations, among other biological effects.[15] TGF-β plays an important role in the differentiation and PC coverage of endothelial cells (EC) in the tumor vascular bed and does so by activating a complex signaling pathway that is illustrated in Scheme 1. TGF-β binds to type I and type II receptors; the former propagates TGF-β signal transduction through Smad proteins. The binding of TGF-β leads to phosphorylation and activation of type I receptor, which contains an intracellular kinase domain that further phosphorylates Smad2 and Smad3. The phosphorylated pSmad proteins subsequently complex to Smad4 to form a transcriptional activation complex that is responsible for the expression of genes in PC differentiation, EC coverage, and blood vessel stabilization.[16,17] Based on this vascular biology, intervention in the TGF-β signaling pathway presents a promising opportunity to achieve vascular access and delivery of cancer drugs and nanocarriers to the tumor site.[7] This can be achieved in a number of ways, including the use of receptor kinase inhibitors.[16] Vascular access can also be improved by reducing the collagen content of the stroma through the use of antifibrogenic drugs, such as losartan (a clinically approved angiotensin II receptor antagonist), targeting stromal fibroblasts and stromal depletion.[18]

Against this background, we hypothesized that an integrated nanotherapy approach could potentially achieve two objectives in PDAC drug delivery, namely, a carrier that targets the stroma to gain vascular access, followed by a carrier that delivers GEM to the tumor site. Such an engineered approach can be accomplished by separate waves of therapy, in which the first wave targets PCs' coverage of the tumor vasculature through delivery of a small molecule inhibitor of TGF-β receptor kinase, followed by a second GEM-delivering carrier that is able to deliver a therapeutic drug load (Scheme 1). In this article, we show the development of a copolymer-coated mesoporous silica nanoparticle (MSNP) carrier that could be used for high efficiency molecular attachment of LY364947, a small molecule inhibitor of the TGF-β signaling pathway (TGFβi). Our research demonstrates that delivery of the inhibitor to the PDAC vasculature is capable of interfering in PC recruitment and EC coverage within 2 h of injecting the TGFβi-MSNP. This allowed access of second-wave nanocarriers (liposomes and MSNPs) at the tumor site. We could also show a dramatic increase in the uptake of a liposome with high GEM loading capacity to the PDAC xenograft sites in animals receiving prior injection of TGFβi-MSNP. This leads to effective PDAC shrinking in a xenograft model and provides proof-of-principle testing for dual-wave *in vivo* therapy. We propose that this engineered approach can also be considered for a range of additional cancers in which the tumor stroma and other inferring biological components result in heterogeneous treatment effects in the tumor microenvironment.

RESULTS

Development of an Efficient MSNP Carrier through Molecular Complexation of a TGFβi. The highly coordinated action of various growth factors contributes to the formation and stabilization of tumor blood vessels.[19] This includes an important contribution by TGF-β, which controls various processes involved in vessel maturation, EC migration, PC differentiation, PC coverage of EC, and determining the permeability of tumor blood vessels.[19−21] A number of small molecule inhibitors have been developed to interfere in the TGF-β signal transduction pathway, including SB505124, LY580276, LY550410, and LY364947.[22] LY364947 is a heterocyclic nitrogenous compound (Figure 1A), which acts as a

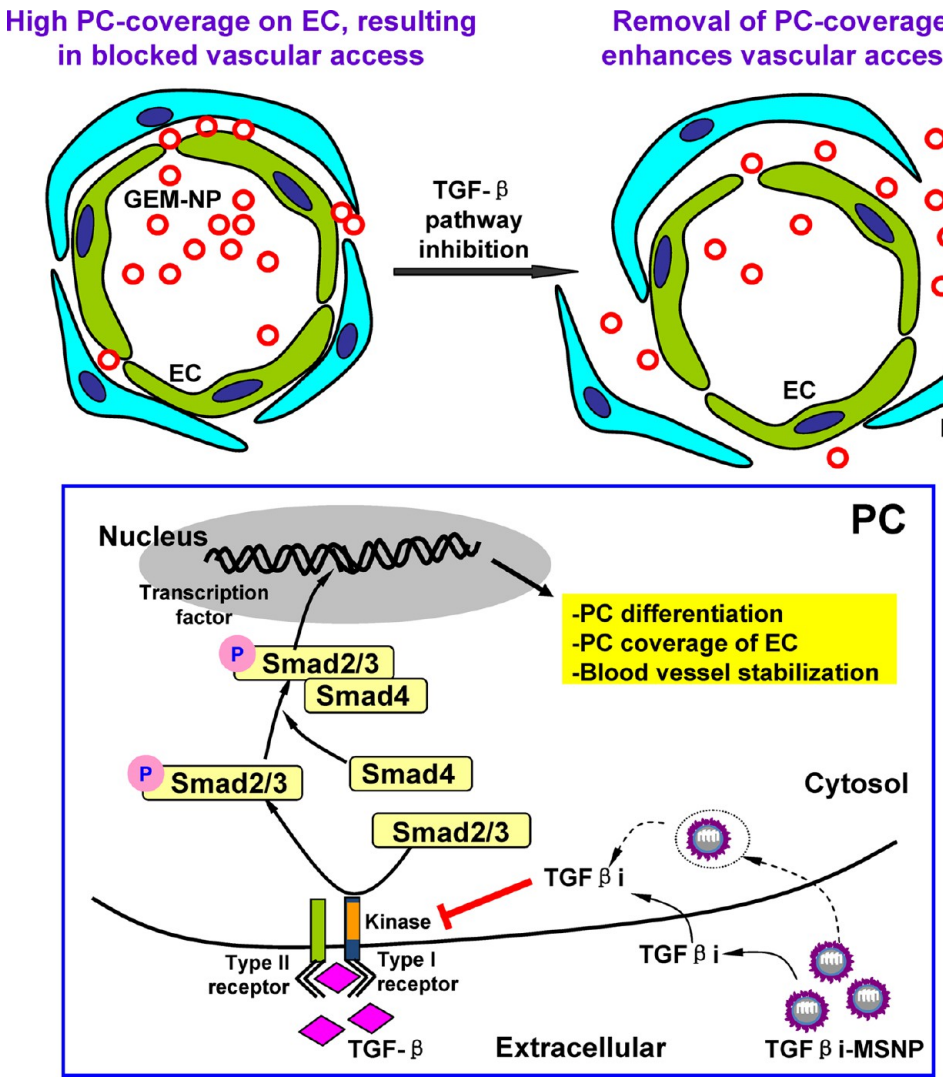

Scheme 1. Role of TGF-β signaling pathway in PC biology and the effects of inhibiting this pathway on drug delivery in the PDAC.[64,65] TGF-β plays an important role in the differentiation and PC coverage of EC in the tumor blood vessels. This role is achieved by a complex signaling pathway as shown in this scheme. TGF-β binds to type II and type I receptors; the latter propagates TGF-β signal transduction by activation of a Smad signaling cascade. Upon binding, the phosphorylated type I receptor, which contains an intracellular kinase domain, further phosphorylates Smad2 and Smad3. The phosphorylated pSmad proteins subsequently complex to co-Smad element, Smad4. The Smad complex is transported into the nucleus, where it interacts with DNA and transcription factors to form a transcriptional activation complex, which is responsible for the expression of genes in PC differentiation, EC coverage, and blood vessel stabilization. LY364947, a small molecule that inhibits type I receptor kinase activity and prevents the activation of Smad2/3, is systemically delivered and released by a MSNP carrier at PDAC tumor site. Due to the acidic pH in the PDAC tumor microenvironment, we expect an acidic stromal pH to contribute to the release of TGFβi. Due to the possible MSNP uptake in PC, another hypothesis is that the TGFβi can be released intracellularly and inhibits TGF-β pathway. Use of LY364947-MSNP as a first-wave particle efficiently decreases PC coverage of the vasculature and allows the IV-injected GEM liposomes find their vasculature access at the PDAC tumor site.

potent inhibitor of the type I receptor-associated Smad kinase *in vitro* and *in vivo*.[7,22,23] Because of its nitrogen display, we could attach LY364947 to a 50 nm MSNP carrier that has been coated with a polyethyleneimine/polyethylene glycol (PEI/PEG) co-polymer. The PEI coating provides a number of non-complexed hydrogens that attach to the nitrogen atom in LY364947 through H-bonding (Figure 1A). PEI-PEG-coated MSNPs are also preferred for systemic inhibitor delivery because these nanoparticles remain monodispersed in biological fluids and have a long circulatory half-life due to decreased opsonization as a result of PEG coating.[24,25] This leads to optimal passive delivery and retention at the experimental tumor site in mice.[24,25] In order to determine the degree of molecular complexation of LY364947 to the MSNP surface, a fixed amount of particles (500 μg) was incubated with incremental amounts (50 to 400 μg) of the inhibitor at 25 °C for a 24 h time period. After washing, spectrophotometric analysis at 269 nm showed an exceptionally good capacity of the coated MSNP to bind to LY364947, culminating in a loading capacity of ~74% w/w (inhibitor/particle) and only a slight increase in particle hydrodynamic size (from

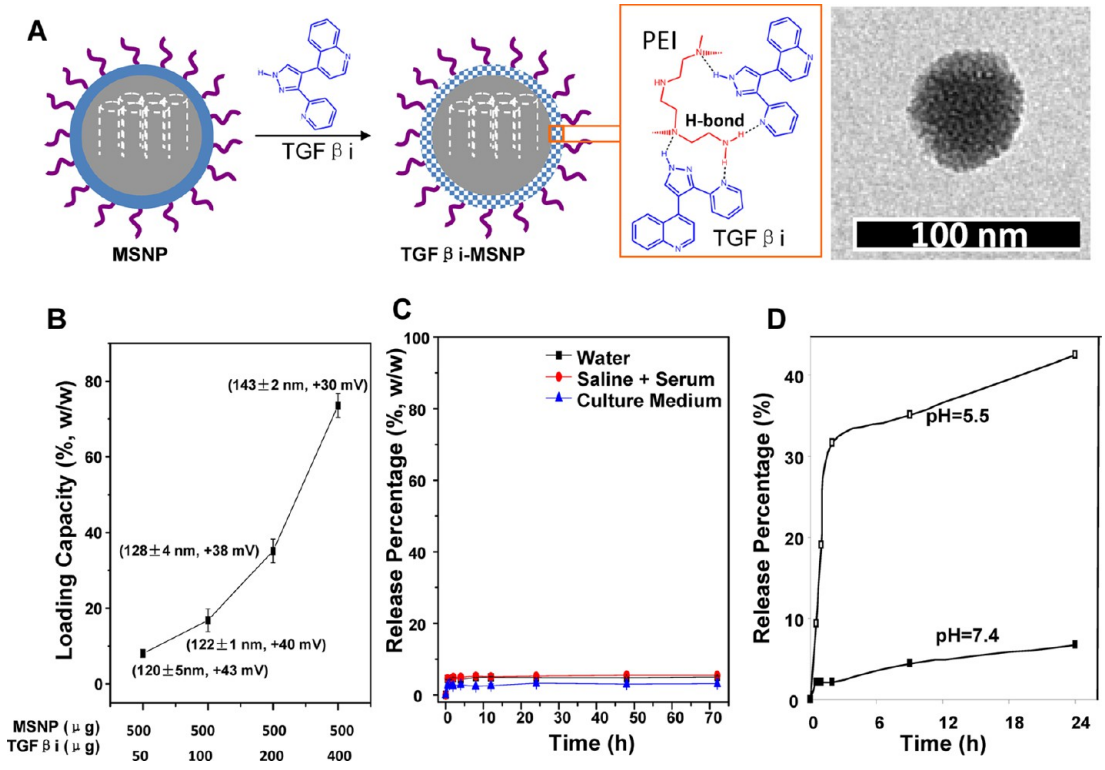

Figure 1. Development of an efficient TGFβi carrier, using molecular complexation to attach LY364947 to PEI-PEG-coated MSNP. (A) Graphical presentation of the particle showing H-bonding of LY364947 to the PEI polymer (see the inset box). We also show a TEM image of the MSNP carrier. (B) Assessment of the maximum loading capacity for LY364947 to the particle. Fixed amounts of the particle (500 μg) were used for incubation with incremental amounts (50−400 μg) of LY364947. The loading capacity (w/w) was quantitatively assessed using the LY364947 OD value at 269 nm. Particle size and ζ-potential in solution were measured by a ZetaSizer Nano and are indicated in brackets. The size and ζ-potential prior to dug attachment were 118 ± 3 nm and +45 mV. (C) Stability of LY364947 attachment in different solutions. The % LY364947 release was studied in deionized water, saline with 2% serum, and DMEM supplemented with 10% FCS at different time points at 37 °C. (D) LY364947 release was studied in pH 5.5 aqueous solution for 24 h and compared with the release profile in PBS (pH 7.4).

120 to 143 nm). This reflects the abundance of H-binding donors on PEI and nitrogen acceptors on the small molecule inhibitor (Figure 1B). While the empty particles exhibited a ζ-potential value of +45 mV in water, LY364947 binding decreased this value to +30 mV (Figure 1B). Figure 1C demonstrates that the drug-bound particles can be stably suspended in water, saline (plus 2% serum) and cell culture medium for 72 h. A subsequent release study showed that LY364947 could be released from the MSNP in a time-dependent manner upon lowering the pH of the solution to 5.5 (Figure 1D). Approximately, 40 wt % of the inhibitor was released within the first 24 h. This release characteristic is relevant from the perspective of a low stromal pH due to increased lactic acid production as a result of glycolysis (Warburg effect).[26]

LY364947-Attached MSNPs Disrupt PC Interactions with EC *in Vitro* and *in Vivo*. To investigate the effects of the TGFβi on co-migration of cultured human vascular smooth muscle cells (phenotypically similar to PC, which shares the same lineage[27,28]) and human microvascular EC, we used a Matrigel assay[27] to compare the effect of nanocarrier to free inhibitor. Figure 2A, in which ECs and PCs were stained with CellTracker Green and CellTracker Red, respectively, demonstrate that the percent of PC/EC colocalization was significantly decreased by TGFβi delivery through the nanocarrier as compared to the effect of free inhibitor (at 1 μM). Representative fluorescent images of the cellular co-migration are shown on the right-hand side of the figure. Upon ligation of the type I receptor by TGF-β, the TGF-β receptor kinase phosphorylates the post-receptor Smad2 and Smad3 proteins (Scheme 1).[29] Looking at Smad2 phosphorylation in PCs by using an immunoblotting approach to discern FITC-conjugated anti-pSmad2,[30] this demonstrated efficient and sustained inhibition of Smad2 phosphorylation for up to 24 h in PCs treated with TGFβi-MSNP compared to cells exposed to free inhibitor only (suppressing pSmad2 for 6 h) (Figure 2B). Quantitative assessment of the green fluorescence intensity by ImageJ software confirmed a statistically significant and sustained inhibition of Smad2 phosphorylation by TGFβi-MSNP (Figure 2C).

In order to determine whether TGFβi delivery to the PDAC tumor site will exert the same effect, we established BxPC3 xenografts in nude mice. These xenografts are known to elicit a dense infiltrating stroma, which surrounds nests of cancer cells and also covers tumor blood vessel fenestrations.[31] The presence of a

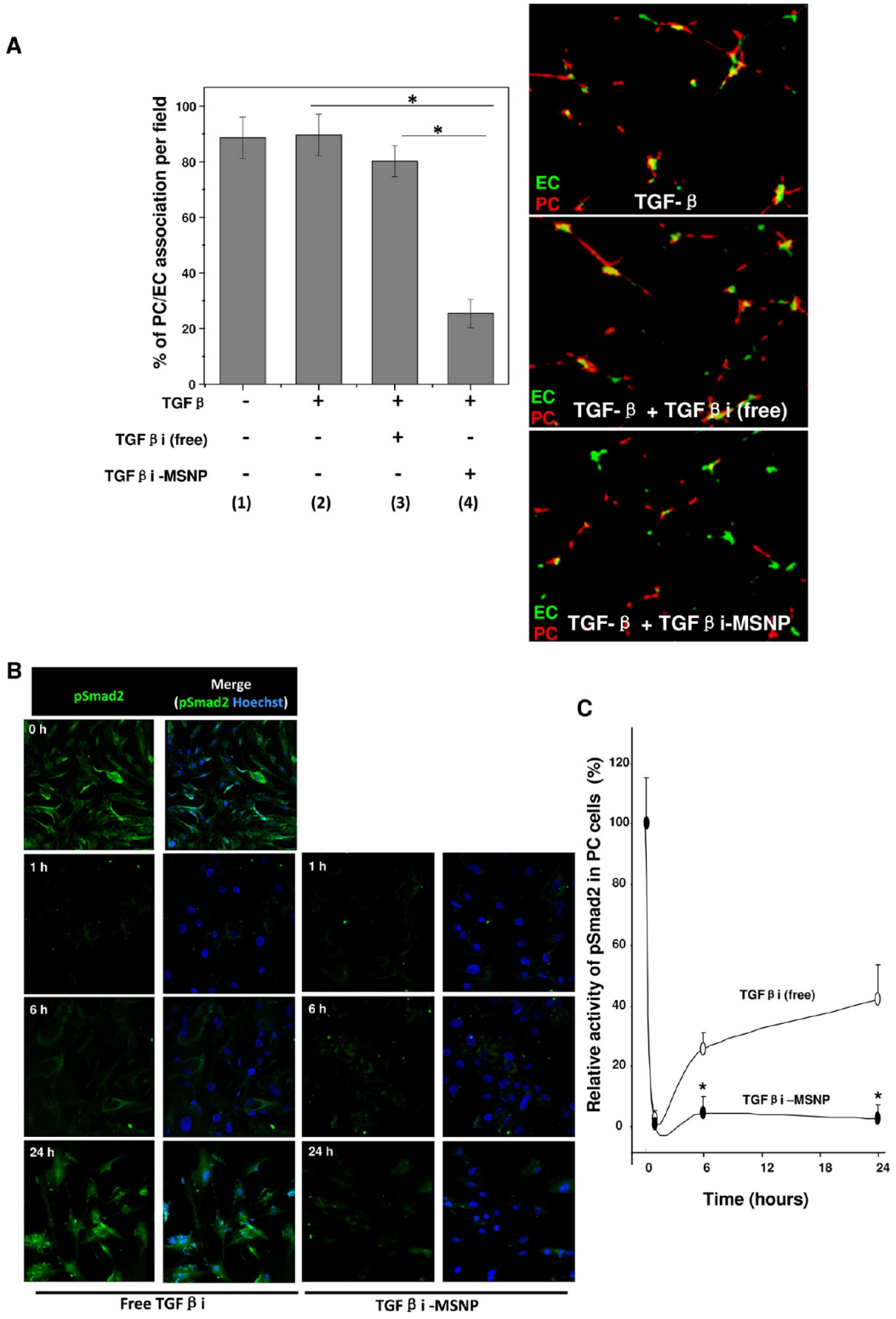

Figure 2. Use of a Matrigel coculture assay and immunofluorescence microscopy to show dissociation of PC binding to EC by TGFβi-MSNPs. (A) HDME (10^4 cells/mL) and HSM cells (5×10^3 cells/mL) were stained with green and red fluorescent markers, respectively. ECs were treated with 2 ng/mL of TGF-β for 3 h, and PCs were treated with free TGF-β or TGFβi-MSNP at inhibitor dose of 1 μM for 3 h. Subsequently, both cell types were cocultured in Matrigel-coated plates for 16 h at 37 °C. PC/EC adhesions were quantitatively determined in five fields using fluorescence microscopy (Zeiss, Germany); *$p < 0.05$. (B) Use of fluorescence microscopy to determine the level of Smad2 phosphorylation. PCs were treated with 2 ng/mL TGF-β for 3 h. Subsequently, the cells were treated with TGFβi-MSNP at an inhibitor dose of 1 μM for 1−24 h. For comparison, free LY364947 was used to treat cells at the same dose. These cells were stained with primary anti-pSmad2 antibody that was detected by a FITC-conjugated secondary antibody. The nucleus was stained by Hoechst 33342. (C) Signal intensity of the green channel, reflecting activated Smad2 (pSmad2), was calculated, using Image J software (version 1.37c, NIH); *$p < 0.05$.

dense stroma in our animal model after 25 days was confirmed by Masson's trichrome staining, which shows heavy collagen deposition in the BxPC3 tumor site (Figure 3A). To achieve effective LY364947 delivery, we made use of the previously demonstrated biodistribution properties and circulatory half-life of the PEI/PEG-coated MSNPs.[24,25,32] The TGFβi-MSNP nanocarriers were freshly prepared at 50% inhibitor/particle ratio before the animal experiment. TGFβi-MSNP was injected intravenously at an inhibitor dose of 1 mg/kg (delivered by 2 mg/kg MSNP) in nude mice expressing tumors ranging from 0.8 to 1.0 cm in diameter. Tail vein injections of saline or the free inhibitor (at the same dose) were used as controls. To demonstrate what impact the inhibitor may exert on PC/EC colocalization, dual-color immunohistochemistry was used to detect EC (FITC-conjugated antibody, recognizing CD31) and PC (Alexa Fluor 594-conjugated antibody, recognizing NG2) fluorescence (Figure 3).[7] This demonstrated that IV-injected TGFβi-MSNP could disrupt the composite (yellow) fluorescence staining that results from the merging of green (EC) and red (PC) fluorescence (Figure 3B). No separation of the green and red fluorescence distribution was observed in saline-treated animals, while injection of the free inhibitor resulted in a slight but nonsignificant reduction of the composite fluorescence staining pattern (Figure 3B). We could observe the presence of the MSNP nanocarrier in the tumor vasculature by electron microscopy; this demonstrated the presence of monodispersed, porous nanoparticles in small tumor blood vessels (Figure 4). Additional TEM images are shown in section S1 in the Supporting Information. Drug release at this site is likely promoted by the anoxic conditions and drop in pH at the tumor site and in the stroma.[26]

All considered, above data provide proof-of-principal testing that complexation of LY364947 to the MSNP surface can be used to target the PDAC stromal barrier and potentially useful for promoting vascular access to the tumor.

LY364947-Bound MSNPs Improve PDAC Access of IV-Injected "Hard" and "Soft" Nanoparticles in BxPC3 Xenografts. Since PCs regulate capillary blood flow as well as vascular access, we asked whether TGFβi-MSNP could improve the egress of nanocarriers at the BxPC3 xenograft site.[33] Two types of particles were used for this biodistribution study, namely, fluorescent labeled "hard" (120 nm PEI-PEG-coated MSNP) and "soft" (137 nm liposome) nanocarriers. These second-wave MSNPs and liposomes were designed with near-infrared (NIR) tags to provide high photon penetration in animal tissues, as previously described by us.[24,25] Detailed characterization of the particles is described in section S2 in Supporting Information, while TEM or cryoEM images are shown in Figure 5A,B. To visualize tumor growth, BxPC-3 cells were stably transfected with a luciferase vector to obtain bioluminescence images in mice following intraperitoneal (IP) injection of D-Luciferin (Figure 5A,B, first row). Baseline images showed very low NIR background in the nontreated tumor-bearing animals (Figure 5A,B, second row). Subsequently, these animals were IV-injected with TGFβi-MSNP (containing 1 mg/kg of the inhibitor), followed after a 2 h interval, by IV injection of 50 mg/kg NIR-labeled MSNPs or liposomes. The biodistribution of these materials was compared to mice in which IV injection of NIR-labeled MSNP was performed without prior administration. NIR fluorescence images, captured at different time points, are shown in the third and fourth rows in Figure 5A,B (the full panel of NIR images is shown in section S3 online). In the absence of prior administration, labeled MSNPs were mostly distributed to the liver, spleen, and kidney in the first 24 h (Figure 5A, first column). Although PEI-PEG-coated MSNPs were optimized for effective biodistribution and passive delivery to non-PDAC tumors,[24,25] there was limited egress in stroma-rich BxPC3 xenografts (Figure 5A, first column). In contrast, in mice injected with TGFβi-MSNP, there was prominent particle uptake in the xenograft sites by 24 h, suggesting enhanced vascular access (Figure 5A, second column). Software analysis of the NIR fluorescence intensity at different time points demonstrated that prior TGFβi-MSNP administration resulted in a significant increase in the fluorescence intensity by 40 h. This signal was sustained for at least 60 h (Figure 5A, lower panel). Very little change in fluorescence intensity was observed in the tumor tissues of mice receiving NIR-MSNP alone. Similar enhancement of tumor uptake by a second hydrothermally synthesized 50 nm MSNP (decorated with quaternary amines and PEG) could be seen at the xenograft site following first-wave TGFβi-MSNP administration (section S4 in the Supporting Information).

In parallel experiments, we assessed the effect of TGFβi-MSNP on the biodistribution of a liposomal carrier (DPPC/cholesterol/DSPE-PEG = 7:2:1) to the BxPC3 xenograft site. Detailed information about liposome synthesis and characterization is available in Supporting Information S2. For ease of particle imaging in mice, a NIR-labeled liposome was developed by incorporating Dylight 680-DMPE (<0.1%, w/w) into the lipid mixture. Compared to the biodistribution of the IV-injected liposomes alone (Figure 5B, first column), there was a significant increase in fluorescence intensity at tumor sites in mice injected with TGFβi-MSNP (Figure 5B, second column). Interestingly, the liposomes accumulated at the tumor site with more rapid kinetics than MSNP (*i.e.*, 1 h post-IV injection). These images also demonstrate a faster rate of disappearance of the liposomes compared to the silica nanoparticles. The more rapid removal kinetics of the liposomes is likely due to their increased degradation rates *in vivo* as well as reduced mechanical stiffness as compared to MSNP (Figure 5B and Supporting Information S5). Similar to

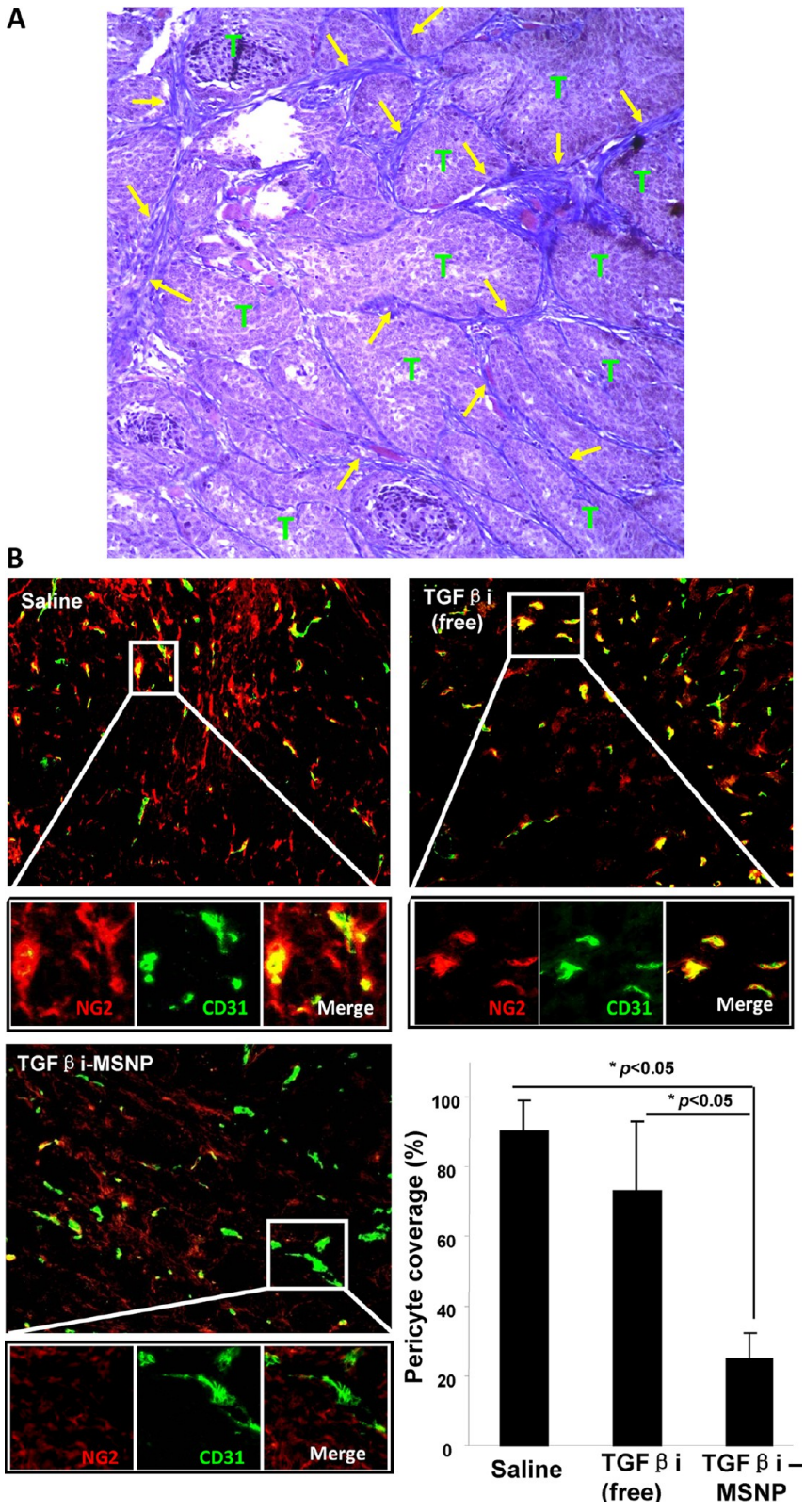

Figure 3. Immunohistochemistry staining of BxPC3 xenograft sections to show TGFβi-MSNP disrupting PC interactions with EC. (A) Staining with Masson's trichrome to show prominent interstitial collagen deposition (in blue). "T" indicates tumor cells. Arrows are pointing to the stroma. (B) Tumor-bearing animals were divided into two groups and received IV-injected TGFβi-MSNP at an inhibitor dose of 1 mg/kg (MSNP dose of 2 mg/kg). Saline and IV injection of the same dose of the free inhibitor were used as controls. Tumor tissues (0.8−1 cm diameter) were collected 1−2 h post-injection and OCT embedded for frozen section and dual-color immunohistochemistry staining. The EC marker (CD31) was labeled green (FITC), and the PC marker (NG2) was labeled red (Alexa Fluor 594). Further image magnification shows the extent of PC/EC colocalization in each group. PC coverage of EC was quantified in three random fields in each group; *$p < 0.05$.

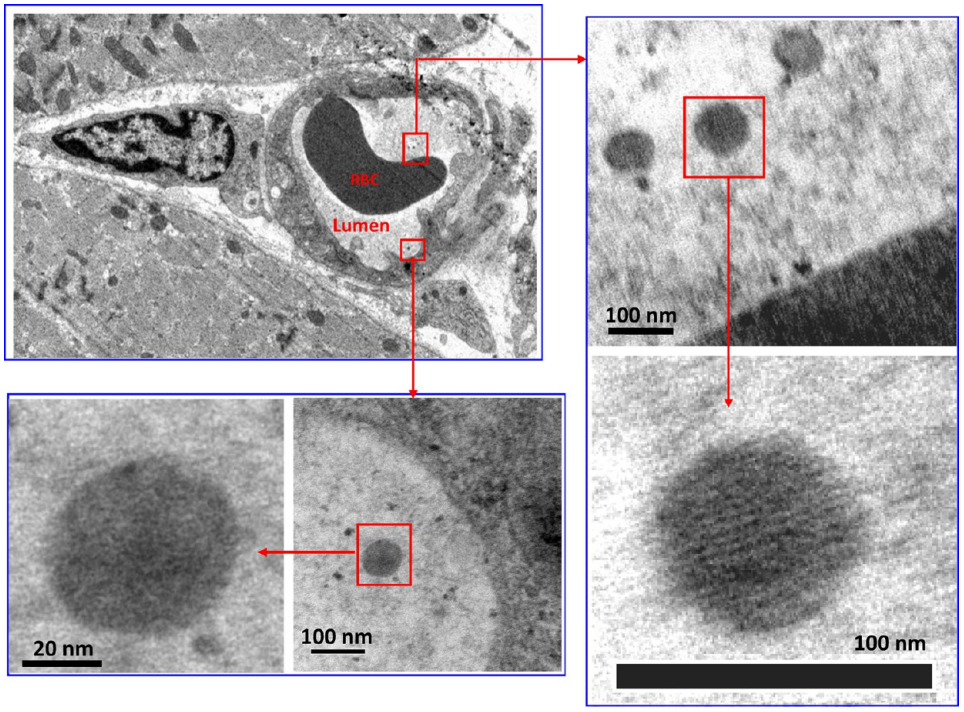

Figure 4. TEM ultrastructural analysis to elucidate the presence of TGFβi-MSNP in BxPC3 xenografts. Electron microscopy to determine the ultrastructure of the tumor 2 h after administration of TGFβi-MSNP. RBC denotes red blood cell. The porous structure of the nanocarrier can be seen inside the tumor blood vasculature. Additional TEM images are displayed in Figure S1.

MSNPs, semiquantitative imaging analysis showed that TGFβi-MSNPs significantly increased liposome retention at the tumor site compared to injecting the liposomes alone (lower panel of Figure 5B).

The mice receiving the NIR-labeled MSNPs were sacrificed at 60 h post-injection, and *ex vivo* fluorescence images were obtained for tumor tissue as well as major organs (Figure 5C, upper panel). Consistent with the live animal imaging data, prior TGFβi-MSNP treatment was associated with increased fluorescence intensity in tumor tissue compared to animals receiving the second-wave treatment alone. Both animal groups showed abundant particle distribution to the liver, spleen, lung, and the kidney. Following *ex vivo* imaging, the collected organs were weighed and used for Si elemental analysis by inductively coupled plasma optical emission spectrometry (ICP-OES). This allowed quantitative analysis of particle distribution, expressed as a percentage (%) of the total mass of administered particles. While ~7% of the particles could be seen to be retained at the tumor site at 60 h in animals treated with TGFβi-MSNP, this amount increased at least 10-fold compared to animals receiving the NIR-MSNP alone (Figure 5C, lower panel). As a result of the shorter retention time for liposomes, the experiments in Figure 5B were repeated in a separate batch of animals in which the tumor tissue and organs were harvested at 24 h to perform *ex vivo* imaging. Consistent with the live imaging results, prior treatment with TGFβi-MSNP significantly increased fluorescence intensity at the tumor site compared to animals injected with liposomes alone. Both groups showed abundant distribution to the liver, spleen, lung, and kidney (Figure 5D, upper panel). Please notice that no NIR signal could be obtained in brain tissue following two-wave treatment. Calculation of fluorescence intensity, using our established protocol,[25] demonstrated that prior treatment with TGFβi-MSNP leads to the retention of ~7% of the administered liposomes as compared to ~1.8% of the injected dose in animals not receiving the inhibitor. This amounts to a 4-fold increase (Figure 5D, lower panel).

TGFβi-MSNPs Improve the Extent of Liposome Intratumoral Distribution in BxPC3 Xenografts. In order to determine whether two-wave therapy changes the biodistribution inside the tumor, Texas-red-labeled liposomes were IV-injected into BxPC3 tumor-bearing mice in the absence or presence of prior TGFβi-MSNP treatment. Visual inspection of the fluorescence distribution under low magnification demonstrated a rim-like distribution of the injected liposomes in animals not receiving any inhibitor treatment (Figure 6A, upper left panel). This distribution is characteristic of the rim-like particle distribution in human xenograft models (*e.g.*, colorectal, breast, and prostate cancer) in mice, in which a spatially heterogeneous particle distribution and high tumor rim particle content have been reported.[34−37] High-magnification images further demonstrated that the liposomes could be visualized as fluorescent intracellular dots in the cytosol and perinuclear regions (Figure 6A). We expect that some of these liposomes are taken up in acidifying endosomal

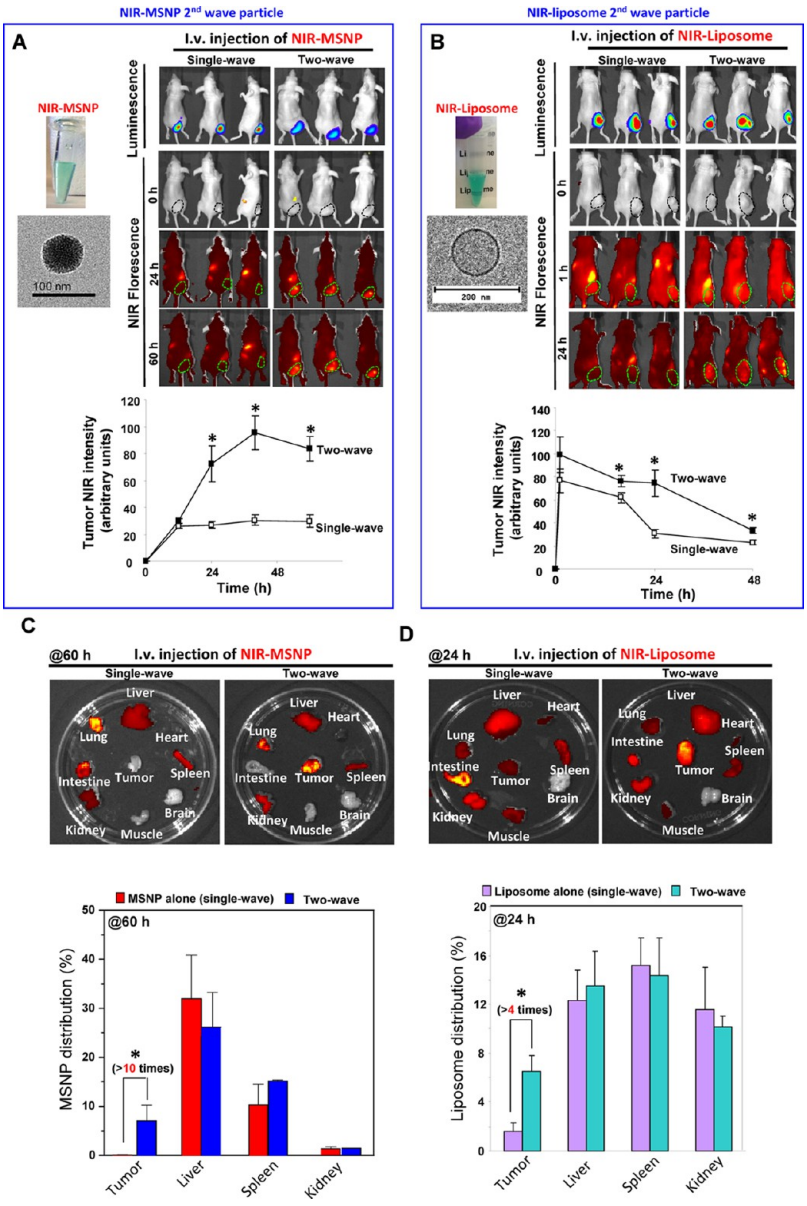

Figure 5. TGFβi-MSNP improves access of IV-injected "hard" and "soft" nanoparticles in BxPC3 xenografts. (A,B) IVIS optical imaging system was used to study the biodistribution of the NIR-labeled particles in BxPC3 tumor-bearing mice. To visualize the luciferase expression at the cancer site, anesthetized mice received IP injection of 75 mg/kg D-Luciferin, followed by collecting the bioluminescence images. Reference fluorescence images were captured before treatment. The tumor-bearing animals were first treated by IV injection of TGFβi-MSNP (inhibitor: 1 mg/kg) followed after a 1−2 h interval by IV injection of 50 mg/kg NIR-labeled PEI-PEG-MSNPs or NIR-liposomes. The *in vivo* biodistribution was compared with the mice receiving IV injection of 50 mg/kg NIR-labeled particles alone. A full panel of NIR images at different time points is shown online in Supporting Information, S3 and S5. Software analysis of NIR fluorescent intensities at different time points and shown in the lower panel in (A) and (B). Filled boxes are two-wave, and open boxes are single-wave; *$p < 0.05$. (C,D) For PEI-PEG-MSNP, 60 h after injection, the animals were sacrificed and tumor tissues as well as major organs collected for *ex vivo* imaging. ICP-OES was used to quantify the Si abundance in the major target organs using our established procedure.[24] As a result of the shorter retention time of liposomes, we repeated the experiments in (B) by harvesting the tumor tissue and organs after 24 h for *ex vivo* imaging. Approximately 100 mg of tumor, spleen, liver, and kidney tissue was weighed out accurately, washed, and homogenized, and the fluorescence intensities per unit amount of each organ were measured by a microplate. The biodistribution of each particle was expressed as percent of total particle dose that was distributed to individual organs; *$p < 0.05$, two-wave compared to use of particle alone.

compartments in tumor cells.[38] In contrast, there was a dramatic change in the intratumoral distribution of liposomes injected after first-wave delivery of TGFβi-MSNP (Figure 6A, upper right panel). Additional immunohistochemical staining to localize CD31 with a FITC-conjugated antibody and NG2 with a pacific-blue-conjugated antibody, allowed us to determine liposomal localization in relation to ECs and PCs (Figure 6B). Compared to single-wave liposomal administration, two-wave treatment resulted in more

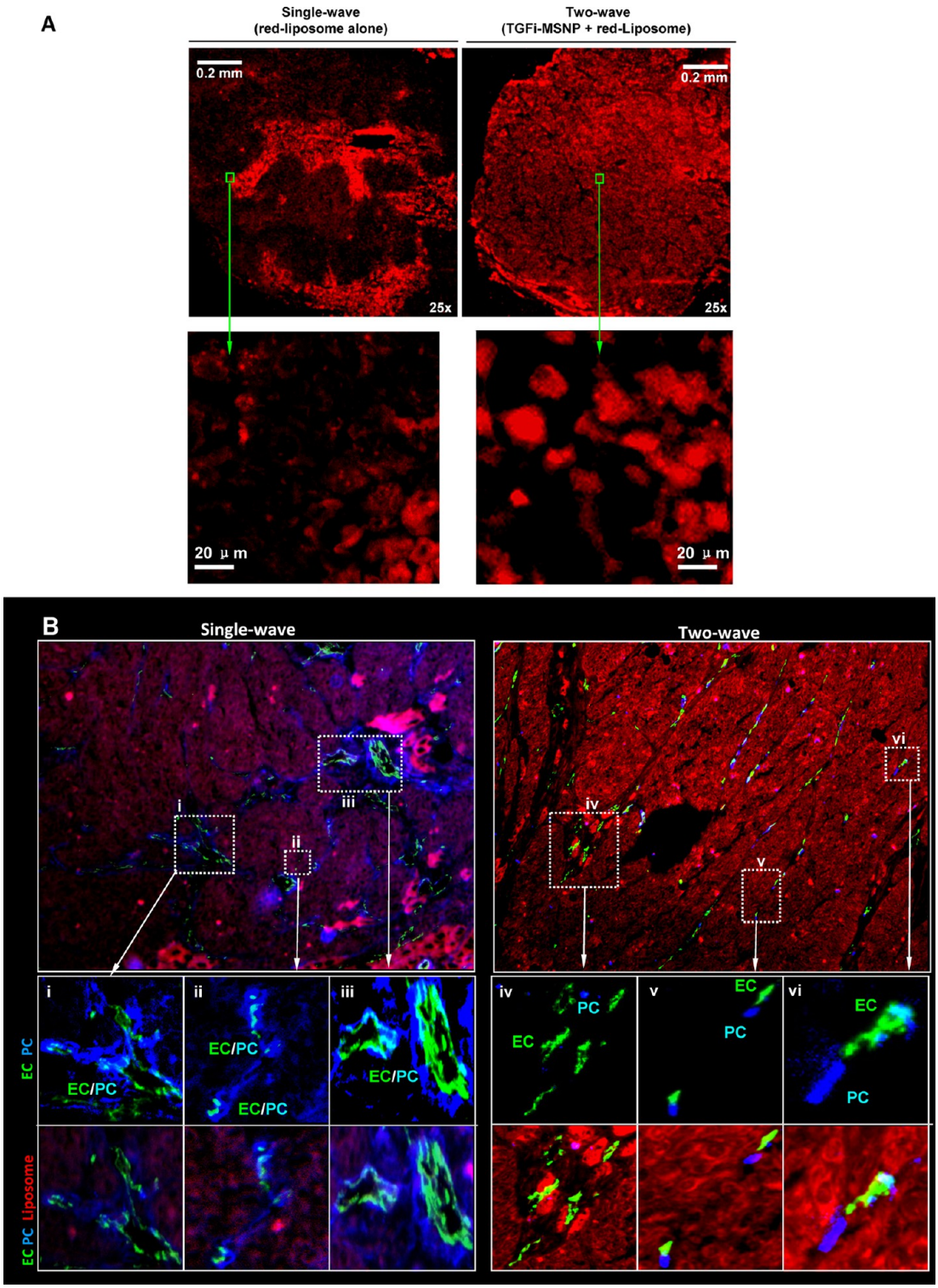

Figure 6. Fluorescent images of tumor tissue sections to show that TGFβi-MSNPs improve the extent of liposome intratumoral distribution in BxPC3 xenografts. (A) BxPC3 tumor-bearing mice received IV injection of TGFβi-MSNP (inhibitor dose: 1 mg/kg; MSNP dose: 2 mg/kg) followed by IV injection of 50 mg/kg Texas-red-labeled liposomes. Tumor tissues were collected 5 h post-liposome injection and embedded in OCT for frozen section. Slides were visualized under a fluorescence microscope. The liposome biodistribution in the tumor section was compared with the mice receiving IV injection of 50 mg/kg Texas-red-labeled liposomes alone. (B) Higher level magnification to show the localization of the liposomes in the tumor in relation to EC (CD31) and PC (NG2) fluorescent markers. CD31 was visualized by a FITC-conjugated secondary antibody and a NG2 by pacific-blue-conjugated secondary antibody. The fluorescent signal from the Texas-red-labeled liposomes was captured in the same view. Zoom-in images, labeled as i–iii, were obtained in an animal injected with liposomes alone, while iv–vi represent images from animals receiving two-wave therapy (lower panel).

abundant and homogeneous liposome distribution in the xenograft tissue. Moreover, merging of blue and green fluorescent images demonstrated the disappearance of EC/PC colocalization during two-wave treatment (Figure 6B, regions "iv", "v", and "vi"). This stands in contrast to the effective colocalization of these cells (Figure 6B, regions "i", "ii", and "iii") in animals injected with liposomes in the absence of the inhibitor. All considered, these data demonstrate that TGFβi-MSNP pretreatment allows vascular access and homogeneous intratumoral distribution of engineered nanoparticles. This prompted the question of whether two-wave therapy can be used to improve the efficacy of GEM delivering to the PDAC tumor site.

Two-Wave Treatment Improves the Efficacy of Gemcitabine Delivery to BxPC3 Tumors. To demonstrate the possible therapeutic benefit of TGFβi-MSNP in the treatment of BxPC3 xenografts, we looked at whether it is possible to trap GEM in the pores of these particles, providing us with a dual delivery nanocarrier such as we demonstrated for doxorubicin and Pgp siRNA in a breast cancer xenograft model.[25] However, different from doxorubicin, we could not achieve sufficient GEM retention in MSNP pores and therefore decided to develop a liposome carrier instead (Figure 5B). The drug-loading capacity of the liposome was optimized by entrapping $(NH_4)_2SO_4$ in the included central volume in the liposome.[39] This allowed free and lipophilic GEM to diffuse through the liposomal membrane, whereupon the protonation inside the liposome leads to GEM retention (Supporting Information S2).[39−42] We optimized the GEM loading procedure by systemically varying the loading time, transmembrane salt gradient, extent of salt washout, temperature, and amount of free GEM offered for loading (Supporting Information S2). This allowed us to achieve a GEM loading capacity of 19.8% w/w, which is much higher than the loading capacity that can be achieved with conventional methods. Full details about the liposome design, detailed physicochemical characterization, optimization of drug loading, stability check, cellular uptake, and ability to protect the drug against cytidine deaminase (CDA) inactivation are described in section S2 in the Supporting Information.

Xenograft-bearing nude mice were IV-injected with 101 mg/kg of the liposomes (GEM dose: 20 mg/kg) 1−2 h after the IV injection of TGFβi-MSNP (TGFβi dose of 1 mg/kg). This paired set of injections was repeated every 3−6 days for 38 days (Figure 7A). The controls included animals injected with saline, free GEM, empty liposomes, TGFβi-MSNP alone, or GEM liposomes alone. Because our previous studies have shown that the empty MSNP carrier lacks anticancer activity,[24,25] we did not include this negative control. Since the free inhibitor resulted in less potent effects in the Matrigel assay and did not significantly affect PC blood vessel coverage in xenografts (Figure 3B), we did not include the free inhibitor in the efficacy experiment for logistic reasons. When comparing the effect on tumor size, the GEM liposomes showed a significantly higher rate of tumor shrinkage than the free drug (Figure 7A). This effect was further enhanced by two-wave treatment but could only be seen beyond 25 days. This delay likely reflects the effect of tumor stage on stroma development. No tumor inhibition was found with saline treatment, TGFβi-MSNP alone, or the use of empty liposomes (Figure 7A).

Two-Wave Therapy Reduces the Systemic Toxicity of GEM. The safety of the nanocarrier delivery system is of key importance, including the inherent safety of the delivery vehicle as well as the encapsulated drug. Safety assessment was performed by monitoring total body weight, blood chemistry, and histological examination of major organs. Compared to saline-treated tumor-bearing mice, no significant body weight changes were observed during the administration of empty liposomes, GEM liposomes, or paired TGFβi-MSNP/GEM liposomes delivery. In contrast, animals receiving free GEM administration showed reduced weight gain (Figure 7B). While none of the animals showed a significant elevation of biomarkers associated with target organs (Supporting Information S6), free GEM resulted in some nephrotoxicity.[43] This manifested as glomerular swelling and edema of Bowman's space in renal glomeruli (Figure 7C). This histological change was not seen in other groups and was not accompanied by urea and electrolyte disturbances. Histological examination of the liver and spleen did not show any gross pathology in any of the experimental groups.

DISCUSSION

In this study, we developed an engineered approach wherein TGFβi-MSNP treatment was used to target the tumor stroma by decreasing PC coverage of tumor vascular fenestrations, followed by the delivery of drug-encapsulating liposomes that could effectively penetrate the tumor site, resulting in enhanced cancer inhibition. In order to achieve optimal *in vivo* efficacy, both the first- and second-wave carriers were designed to prolong circulation time through PEGylation as well as using methods to optimize the drug-loading efficiency. In the case of the copolymer-coated MSNP, a high drug load was achieved through chemical complexation to PEI, from which LY364947 was released to interfere in the TGF-β receptor signaling and subsequent PC differentiation and attachment to EC (Scheme 1). This allowed second-wave nanocarriers access through the open vascular fenestrations, with the ability to increase GEM delivery by a liposome. Optimal liposome design was achieved by using a transmembrane ammonium sulfate gradient to trap GEM inside the liposome. Effective release of the encapsulated GEM throughout the tumor interstitium and cancer cells was associated with enhanced tumor

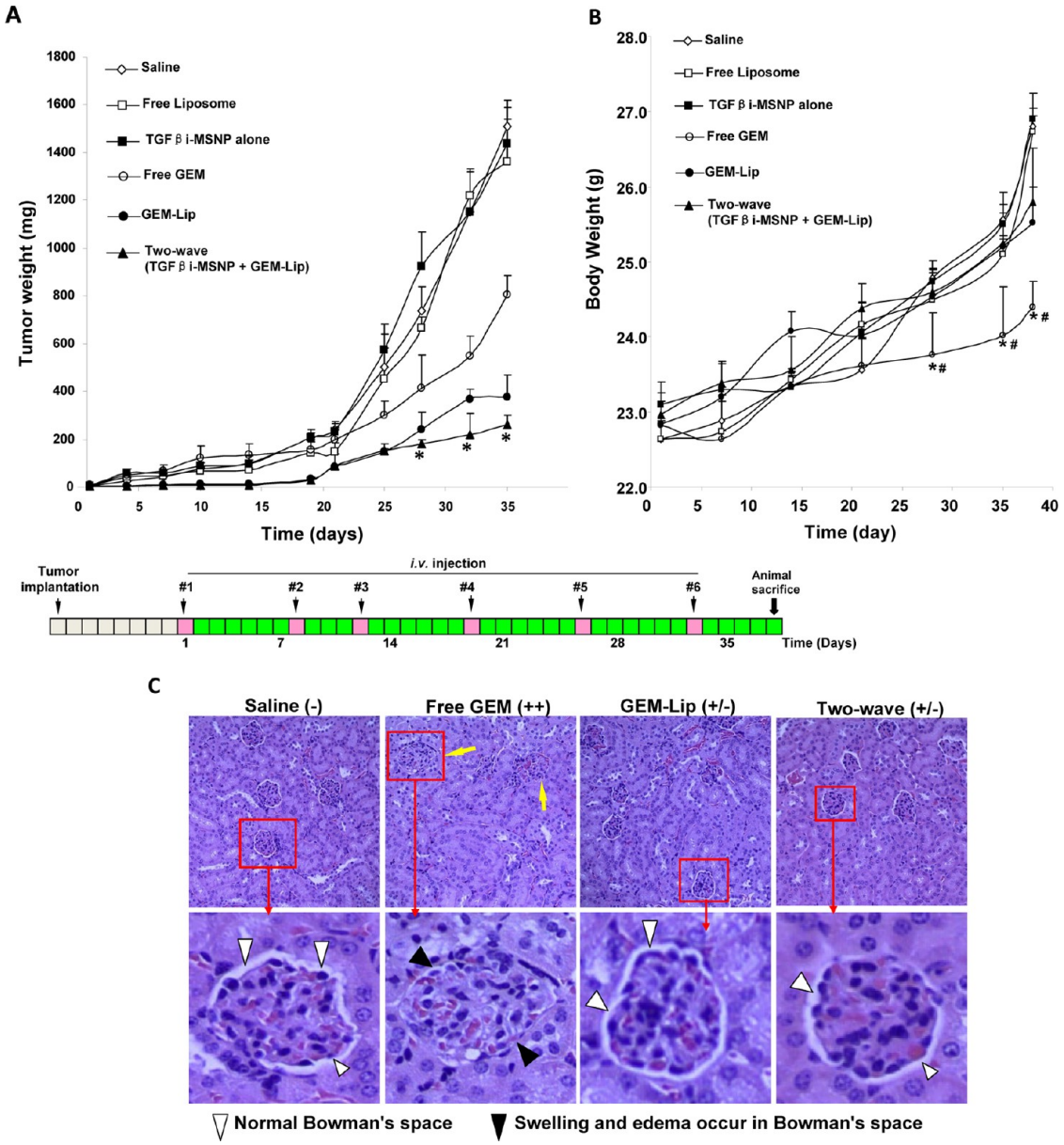

Figure 7. Tumor growth inhibition and assessment of animal weight and kidney histology in BxPC3-bearing mice. (A) Detailed animal treatment procedures are described in the Materials and Methods section. BxPC3 cells were subcutaneously injected into mice 7 days before treatment (gray boxes). Animals then received six IV injections (red boxes) every 3−6 days (green boxes) for 38 days as shown. The effect of two-wave therapy on tumor weight was compared to animals receiving saline, GEM liposome alone, free GEM, empty liposome, and TGFβi-MSNP. Tumor size was measured twice a week. Tumor weight was calculated according to the formula: tumor weight (mg) = (length in mm) $\times$ (width in mm)^2/2;[60−63] *$p < 0.05$, compared to GEM liposome group. (B) Recorded animal weights were expressed for the duration of the experiment; *$p < 0.05$, compared to saline; #$p < 0.05$, compared to GEM liposome. (C) Histological sections were stained with hematoxylin/eosin (H&E) and examined by light microscopy. Representative images are shown. Higher magnification images were also obtained to show the swelling and edema of Bowman's space, representing free drug toxicity. The white arrows point to normal glomeruli, and the black arrows point to swelling and edema in Bowman's space as an indication of free GEM toxicity.

shrinkage and the reduction of GEM toxicity compared to free drug. All considered, these data provide proof-of-principle testing for two-wave nanotherapy that targets the stroma and provides protected delivery of GEM to the tumor site. This advance will now allow us to test the dual-wave approach in a more rigorous orthotopic pancreatic cancer model.

Utilizing our multifunctional MSNP platform to conduct proof-of-principle testing of various human cancer models in mice, a number of biological impediments as well as heterogeneity of the tumor microenvironment have surfaced to challenge nano cancer drug delivery beyond the traditional concept of passive and active delivery. While vascular abnormalities such as large fenestrations could contribute to nanocarrier egress at the cancer site (enhanced permeability and retention effect, EPR effect), there are a number of tumor-specific biological impediments to

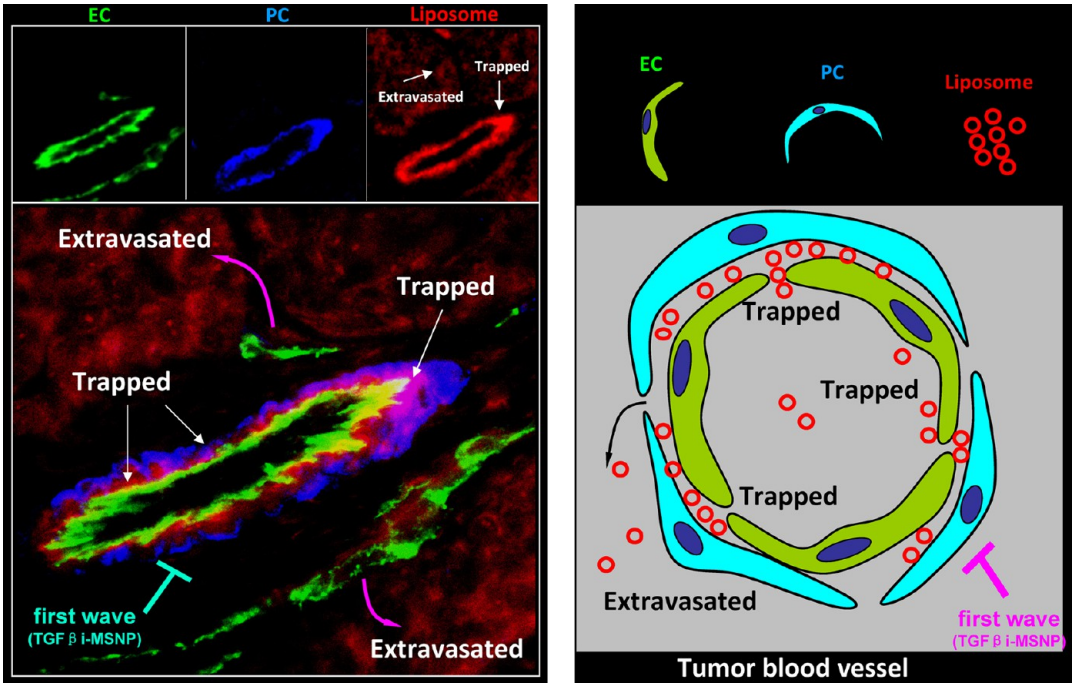

Figure 8. Changing the PC coverage of vascular fenestrations is important for delivery of the liposomal GEM carrier. This fluorescent stained histological section shows that the PDAC tumor uses a dense stromal barrier, which includes PCs blocking the vascular access of IV-injected red fluorescent liposomes. The fluorescence microscopy image obtained from the tumor site of an animal receiving prior TGFβi-MSNP therapy shows a region of a blood vessel where PCs are trapping some liposomes just beyond their point of egress from the vascular fenestrations. In contrast, other blood vessel regions not showing PC coverage allow liposome extravasation to the tumor interstitium and cancer cells.

overcome before achieving homogeneous distribution of the nanocarrier or widespread killing of tumor cells. In the case of PDAC, the display of a dysplastic stroma (which includes PC coverage of vascular fenestrations) is a key consideration (see Figure 8). It is important to consider this barrier in designing a nanocarrier for PDAC drug delivery. One consideration, demonstrated in the current study, is to use an engineered approach that makes use of a primary nanocarrier to provide vascular access by perturbing the stroma, followed by a second nanocarrier that is retained and deliver GEM at the tumor site. This is in agreement with other creative ideas for multistage and combination nanotherapeutics to provide an impact on blood vessel permeability, blood vessel patency, inhibition of drug-inactivating enzymes, and/or target specific biological factors that play a role in the heterogeneity of the tumor microenvironment in multiple cancer types.[7,14,44,45] These include biophysicochemical factors (hypoxia, acidosis, high interstitial fluid pressure) that interfere in drug delivery, heterogeneous cellular components other than cancer cells (endothelial cells and pericytes, cancer-associated fibroblasts, and inflammatory cells), as well as noncellular components (extracellular matrix, matrix metalloproteinase, soluble growth factors and their receptors, and integrins)[46] that could be targeted by an engineered approach. One example is the use of macrolide-modified gold nanorods that were designed to target and activate the antitumor potential of macrophages.[47] This research demonstrated that nanorods preferentially accumulate in tumor-associated macrophages, leading to significant enhanced killing of breast cancer cells.[47] The importance of manipulating the tumor microenvironment is further illustrated by our study in which we achieved enhanced vascular permeability in the stromal barrier through the delivery of a small molecule inhibitor. While we have demonstrated similar, but less prominent, stromal effects in drug-resistant human breast cancer xenografts, microvascular heterogeneity and delivery of the MSNP played an important role in decreasing the effectiveness of the treatment.[25] Since the stromal contribution is accentuated in PDAC, it is less likely that this cancer will be affected by nanocarriers that rely on the EPR effect alone. Based on our discovery, it is reasonable to envisage the development of a number of second-wave systems that carry and deliver a drug, drug combination (*e.g.*, GEM/paclitaxel and FOLFIRINOX), or a drug plus a nucleic acid to treat PDAC. Reliance on an EPR effect is more likely to be effective in tumors with a lesser stroma.[7]

In clinical studies, the idea of targeting the PDAC stroma has been addressed by using PEGylated hyaluronidase PH20 (PEGPH20), which targets a tumor matrix component (hyaluronan) that plays a role in generating high interstitial fluid pressure (IFP). The high IFP interferes in drugs and nanoparticles penetration.[48] Results from an ongoing clinical trial have demonstrated that the combination of GEM with PEGPH20

treatment can improve the stromal barrier, allowing chemotherapeutic agents to freely permeate the cancer site.[49,50] However, this approach differs from our study in which we did not observe a significant change in the collagen content (data not shown) as a result of the relatively short duration of treatment. In a recent phase III clinical trial in untreated PDAC patients with metastatic disease, it has been demonstrated that the combination of Abraxane (paclitaxel/albumin complex) with GEM could induce a statistically significant improvement in overall survival compared to patients receiving GEM alone (median of 8.5 *vs* 6.7 months).[51] In an accompanying animal study, it was demonstrated that paclitaxel is capable of suppressing the desmoplastic stroma and increasing the intratumoral GEM content 2.8-fold as a result of reducing CDA enzyme levels.[44,52] Therefore, it will be interesting to test, in the future, whether combined delivery of GEM and paclitaxel by a nanocarrier could be used as a second-wave therapy that advances PDAC treatment.

The TGF-β superfamily plays an important role in cancer biology.[22] This includes effects in PC interactions with ECs during neo-angiogenesis.[17] Inhibition the TGF-β signaling pathway has been studied in tumor xenograft models, retinal vasculature, and a three-dimensional PC/EC coculture model.[7,17,21,53] Collectively, these studies indicate that TGF-β plays a key role in microvasculature and that inhibition of the TGF-β signaling pathway can disrupt the integrity and function of small blood vessels by dissociating PC interactions with EC.[7,17,21,53] Our results also confirm previous studies showing that intraperitoneal injection of free drug inhibitor promotes vascular access and accumulation of nanoparticles and macromolecules in BxPC3 xenografts and an OCUM-2MLN orthotopic gastric cancer model.[7] TGF-β also suppresses local tumor immune responses, and one can envisage that TGFβi-MSNP could also be used to boost the function of tumor antigen-specific $CD8^+$ T cells by interfering with the immunosuppressive environment.[54,55]

It is important to comment on how TGFβi may be released at the xenograft site. Our hypothesis is premised on *in vitro* release data showing that LY364947 could be released from the MSNP in a time-dependent manner by lowering the pH of the solution to 5.5 (Figure 1D). It is known that the pH value of malignant tumors, including PDAC, is acidic.[26,56] This is due to the increased glucose uptake, glycolysis, and lactic acid production (Warburg effect), which combined with poor perfusion results in an acidic tumoral pH compared to normal tissue (pH 7.2−7.4).[26] The pH classically drops to ~6.5, but can be as low as ~5.5 in mesothelioma xenografts.[57] Moreover, compared to cancers with well-developed vasculature, we expect an even lower pH in pancreatic cancer due to significant hypoxia, presence of a dense stroma, and poor tumor perfusion.[58] While the local pH value in PDAC blood vessels, the stroma, and fenestrations is unknown, lactic acid is also produced in the tumor stroma.[59] The fact that this pH-dependent release may be absent in the noncancerous tissue (*i.e.*, blood brain barrier) could explain why we do not observe a NIR signal in the brain (Figure 5).

Finally, it is worth reflecting on the importance of an optimal loading capacity for drugs encapsulated in or assembled on the nanocarrier. Optimal drug loading is important for efficacious cancer cell killing as well as limiting toxicity by decreasing the amount of nanocarrier and drug that are injected systemically. Loading capacity is also an important consideration for manufacturing purposes. Through the use of efficient molecular complexation, we were able to optimize the attachment of LY364947 to MSNP. Using H-bonding of PEI to the electronegative nitrogen atoms in the inhibitor, we could achieve a 74% (w/w) loading capacity. While it is reasonable to postulate a high loading for other PEI-PEG-decorated particles (including nonporous particles), it would require new and expensive biodistribution studies without a guarantee of safety, good dispersal, and long circulatory half-life. In addition to applications in cancer, the TGFβi-loaded MSNPs could also be useful for the treatment of inflammatory disease, pulmonary fibrosis, and arthritis. In the case of a liposomal carrier, a high loading capacity (~20%) for GEM was achieved by creating an ammonium sulfate gradient across the liposomal membrane, which allowed intraliposomal retention of the drug after protonation.[39] This leads to stabilization of the encapsulated GEM as a gel-like precipitate in the liposome (Supporting Information S2).[39]

CONCLUSION

In conclusion, by addressing a specific, major biological impediment to drug delivery, we developed an engineered approach to the PDAC stromal barrier through a nanoparticle that allows vascular access, thereby facilitating the entry of a liposomal GEM carrier. We propose that this approach should be considered as an important design feature for nanocarriers in addition to traditional consideration of passive and active drug delivery approaches.

MATERIALS AND METHODS

Synthesis of PEI-PEG-Coated Mesoporous Silica Nanoparticles and NIR Labeling. The synthesis of the 50 nm MSNP core was carried out as previously described by us, using a sol−gel chemistry procedure.[24,25] The particle surface was modified using electrostatic attachment of a 1.8 kDa PEI polymer, which was

subsequently used for covalent attachment of 5 kDa PEG. To perform PEI coating, 10 mg of MSNP was suspended in 1 mL of an ethanol solution containing 2.5 mg/mL of PEI of MW 1.8 kDa. The solution was sonicated and stirred for 30 min. The particles were further washed in ethanol to remove excess PEI and trace amounts of surfactant. The PEI-coated particle was subsequently transferred into 1.5 mL of DMF, mixed with 50 mg of activated NHS-poly(ethylene glycol)methyl ether (m-PEG, MW 5 kDa), and stirred for 24 h. The nanoparticles were washed with DMF and ethanol and resuspended in water.[24,25] The NIR fluorescent dye, DyLight 680 NHS ester, was used for particle labeling. Ten milligram particles were suspended in 1 mL of DMF and mixed with 0.1 mg of Dylight 680. The reaction took place under an inert atmosphere during stirring at room temperature for 12 h. The particles were centrifuged and washed with deionized water.[24]

Assessment of TGFβi Loading Capacity and Binding Stability. Various volumes (10, 20, 40, 80 μL) of 5 mg/mL LY364947 in DMSO solutions were mixed with 1 mL of a 0.5 mg/mL MSNP aqueous suspension. The mixed solutions were stirred at 25 °C for 24 h and washed three times with deionized water. After centrifugation at 15 000 rpm for 30 min, the supernatants were collected to obtain LY364947 OD values at 269 nm (M5e, Molecular Devices, USA). The loading capacity was calculated as follows: loading capacity (%, w/w) = total minus non-encapsulated LY364947 by weight/MSNP weight × 100%. In order to determine the stability of LY364947 attachment, the drug release was studied in deionized water, saline containing 2% serum, or DMEM supplemented with 10% serum for time periods ranging from 0 to 72 h at 37 °C. Following sample centrifugation at 15 000 rpm for 30 min, the release percentage was calculated according to the following equation: release percentage = the weight of LY364947 in the supernatants/the total weight of attached LY364947 at $t = 0 \times 100\%$.

Cell Lines and Cell Culture. Human microvascular endothelial cells (HDME) were purchased from ScienCell Research Laboratories (Carlsbad, CA). The ECs were cultured in endothelial cell medium (ECM, Carlsbad, CA) containing 5% FBS, 1% endothelial cell growth supplement (ScienCell, Carlsbad, CA), 100 U/mL penicillin, and 100 μg/mL streptomycin. Human smooth muscle cells (HSM, exhibiting a pericyte-like phenotype[27]) were purchased from American Type Culture Collection (ATCC). The PCs were cultured in ATCC-formulated F-12K medium containing 0.05 mg/mL ascorbic acid, 0.01 mg/mL insulin, 0.01 mg/mL transferrin, 10 ng/mL sodium selenite, 0.03 mg/mL endothelial cell growth supplement, 10 mM 4-(2-hydroxyethyl)-1-piperazine-ethanesulfonic acid (HEPES), 10 mM 2-[(2-hydroxy-1,1-bis-(hydroxymethyl)ethyl)amino]ethanesulfonic acid (TES), and 10% FBS. BxPC3 cells were purchased from ATCC and cultured in Dulbecco's modified Eagle medium (DMEM) (Carlsbad, CA) containing 10% FBS, 100 U/mL penicillin, 100 μg/mL streptomycin, and 2 mM L-glutamine.

Matrigel Assay. To study the effect of TGFβi-MSNP on PC/EC interactions, the Matrigel assay was performed using a modified method.[27] In order to distinguish the PCs and ECs in the Matrigel assay, HDME cells (10^4 cells/mL) and HSM cells (5×10^3 cells/mL) were stained with CellTracker Green CMFDA (Invitrogen, Grand Island, NY) and CellTracker Red CMTPX (Invitrogen, Grand Island, NY) 24 h before the experiment. After the staining, ECs were treated with 2 ng/mL TGF-β for 3 h, and PCs were treated with free TGF-β or TGFβi-MSNP at an inhibitor dose of 1 μM for 3 h. Subsequently, both cell types were cocultured in Matrigel-coated 6-well plates for further incubation of 16 h at 37 °C. PC/EC adhesions were quantitatively determined from five fields obtained from three independent samples with a fluorescence microscope (Zeiss, Germany).

Smad2 Activation Assay. Smad2 activation was determined using immunofluorescent staining in 8-well chamber slides in which 4×10^4 PCs were cultured in each well containing 0.4 mL of culture medium. Sixteen hours post-cell seeding, PCs were treated with 2 ng/mL TGF-β for 3 h. Subsequently, the cells were treated with TGFβi-MSNP at an inhibitor dose of 1 μM for 1−24 h. For comparison, free TGFβi was used to treat the cells at an identical dose. Subsequently, PCs cells were fixed, permeabilized, and stained for pSmad2 with a standard immunocytochemistry protocol. This staining was performed by using a 1:500 dilution of primary anti-pSmad2 antibody (Abcam, Cambridge, MA) for 16 h at 4 °C. This was followed by a 1:500 dilution of a FITC-conjugated secondary antibody (Santa Cruz, CA) for 1 h. The nuclei were stained with Hoechst 33342. Slides were visualized under a confocal microscope (Leica Confocal 1P/FCS). The signal intensity of the green channel, revealing activated Smad2, was calculated by ImageJ software (version 1.37c, NIH).

Establishment of a BxPC3 Tumor Xenograft Model. Athymic BALB/c nu/nu female mice (6 weeks) were purchased from the Charles River Laboratory and maintained under pathogen-free conditions. All animal experiments were performed using protocols approved by the UCLA Animal Research Committee. For tumor visualization in mice using optical imaging, permanent transfection of a luciferase construct by a lentiviral vector was performed in BxPC3 cells. The detailed procedure is described in Supporting Information, S7. To grow tumor xenografts, BxPC3-luc cell suspension (0.1 mL, 5×10^6 cells/mL) was injected subcutaneously in the mice. To determine treatment efficacy, the mice received a series of treatments 7 days post-tumor implantation. For performance of the imaging experiments, the tumor-bearing animals were used 3−4 weeks after tumor implantation, at a stage when tumor size measured 0.8−1 cm.

Biodistribution. Imaging studies were performed to determine the effect of the TGFβi-delivering particle on the biodistribution of secondary nanocarriers to the BxPC3-luc tumor. To visualize the tumor, the mice were IP-injected with 75 mg/kg D-Luciferin, and bioluminescence images were acquired. Subsequently, the mice were IV-injected with TGFβi-MSNP at an inhibitor dose of 1 mg/kg (MSNP dose, 2 mg/kg). One to two hours later, the mice were IV-injected with 50 mg/kg NIR-labeled MSNP or liposomes. NIR fluorescent images were acquired at the indicated time points, using an IVIS Imaging System (Xenogen, Toronto, ON, Canada). This treatment was compared to the mice receiving IV injection of NIR-MSNPs or liposomes alone at 50 mg/kg. The tumor tissue together with major organs (heart, lung, spleen, liver, kidney, brain, and cardiac muscle) was collected and used for *ex vivo* imaging.

Transmission Electron Microscopy of the BxPC3 Tumor in Mice Receiving TGFβi-MSNP Injections. BxPC3 tumor-bearing mice (tumor size: 0.8−1 cm in diameter) were IV-injected with TGFβi-MSNP at an inhibitor dose of 1 mg/kg (MSNP dose, 2 mg/kg). The tumor biopsies were rapidly collected 2 h post-injection, washed in PBS, and immediately fixed with 2.5% glutaraldehyde in PBS at room temperature for 2 h and stored at 4 °C. Further sample preparation and sectioning were performed by the Electron Microscopy Services Center in Brain Research Institute at UCLA. Briefly, after further fixing with 1% OsO_4 in PBS, the samples were dehydrated in a graded ethanol series, treated with propylene oxide, and embedded in resin. Approximately, 60−80 nm thick sections were cut on a Leica ultramicrotome and picked up on Formvar-coated copper grids. The sections were examined in a CM120 electron microscope (Philips).

Determination of EC/PC Colocalization in Tumor Tissues. The tumor tissues were embedded with an OCT reagent before sectioning to provide 4 μm thick slices. The slices were washed three times in PBS and fixed. For EC staining, the sections were first incubated with rat-anti-mouse CD31 monoclonal antibody (1:500) at 4 °C overnight. After removal of the primary antibody and washing in PBS three times, FITC-conjugated goat-anti-rat IgG (1:500) was added and incubated at room temperature for 1 h. For PC staining, the same section was further incubated with primary antibody of NG2 (1:500) at 4 °C overnight and followed by Alexa594- or pacific-blue-conjugated secondary antibody (1:1000) at room temperature for 1 h. All the incubations were performed in the dark. The slices were visualized under a fluorescence microscope. The PC coverage was counted in three randomly selected fields.

Xenograft Studies To Determine the Efficacy of Two-Wave Treatment on Tumor Shrinkage. One week after tumor implantation, the BxPC3 tumor-bearing mice were randomly divided into six groups. These groups were used for comparing the effects of saline, free

liposome, TGFβi-MSNP alone, free GEM, GEM liposome alone, and two-wave treatment. Each animal in the two-wave group received IV injection of TGFβi-MSNP at an inhibitor dose of 1 mg/kg (MSNP dose, 2 mg/kg) followed by a liposome dose of 101 mg/kg (GEM dose, 20 mg/kg) after a 1−2 h interval. Altogether, these animals received six paired injections over a 38 day time period (Figure 6A). The free GEM and GEM-loaded liposome groups received the same drug dose in the absence of TGFβi-MSNP pretreatment. The groups treated with saline, empty liposome, and TGFβi-MSNP were used as controls. The body weight and tumor size were recorded once or twice per week.

For tumor size measurement, the length and width axes of each xenograft tumor were precisely measured to the nearest 0.1 mm by a caliper. Tumor weight was calculated according to the formula: tumor weight (mg) = (length in mm) × (width in mm)^2/2.[60−63] This formula was also used to calculate tumor weight, assuming a tissue density of 1 mg/mm^3. The statistical significance of the changes between two-wave group and GEM liposome group was analyzed using a *t* test (Excel software).

Conflict of Interest: The authors declare no competing financial interest.

Acknowledgment. This study was funded by the U.S. Public Health Service Grant RO1 CA133697. Y.-S.L. and C.J.B. are supported by NCI Cancer Nanotechnology Platform Partnership Grant 1U01CA151792-01.

Supporting Information Available: Additional figures, table, results, and method descriptions as described in the text. This material is available free of charge *via* the Internet at http://pubs.acs.org.

Note Added after ASAP Publication: This paper was published ASAP on October 28, 2013. The abstract graphic and Figure 2 were replaced and the revised version was reposted on October 30, 2013.

REFERENCES AND NOTES

1. Hezel, A. F.; Kimmelman, A. C.; Stanger, B. Z.; Bardeesy, N.; DePinho, R. A. Genetics and Biology of Pancreatic Ductal Adenocarcinoma. *Genes Dev.* **2006**, *20*, 1218–1249.
2. Wray, C. J.; Ahmad, S. A.; Matthews, J. B.; Lowy, A. M. Surgery for Pancreatic Cancer: Recent Controversies and Current Practice. *Gastroenterology* **2005**, *128*, 1626–1641.
3. Kleeff, J.; Reiser, C.; Hinz, U.; Bachmann, J.; Debus, J.; Jaeger, D.; Friess, H.; Büchler, M. W. Surgery for Recurrent Pancreatic Ductal Adenocarcinoma. *Ann. Surg.* **2007**, *245*, 566–572.
4. Erkan, M.; Hausmann, S.; Michalski, C. W.; Fingerle, A. A.; Dobritz, M.; Kleeff, J.; Friess, H. The Role of Stroma in Pancreatic Cancer: Diagnostic and Therapeutic Implications. *Nat. Rev. Gastroenterol. Hepatol.* **2012**, *9*, 454–467.
5. Morikawa, S.; Baluk, P.; Kaidoh, T.; Haskell, A.; Jain, R. K.; McDonald, D. M. Abnormalities in Pericytes on Blood Vessels and Endothelial Sprouts in Tumors. *Am. J. Pathol.* **2002**, *160*, 985–1000.
6. Armulik, A.; Abramsson, A.; Betsholtz, C. Endothelial/Pericyte Interactions. *Circ. Res.* **2005**, *97*, 512–523.
7. Cabral, H.; Matsumoto, Y.; Mizuno, K.; Chen, Q.; Murakami, M.; Kimura, M.; Terada, Y.; Kano, M. R.; Miyazono, K.; Uesaka, M.; *et al.* Accumulation of Sub-100 nm Polymeric Micelles in Poorly Permeable Tumours Depends on Size. *Nat. Nanotechnol.* **2011**, *6*, 815–823.
8. Zhang, L.; Nishihara, H.; Kano, M. R. Pericyte-Coverage of Human Tumor Vasculature and Nanoparticle Permeability. *Biol. Pharm. Bull.* **2012**, *35*, 761–766.
9. Patra, C. R.; Bhattacharya, R.; Wang, E.; Katarya, A.; Lau, J. S.; Dutta, S.; Muders, M.; Wang, S.; Buhrow, S. A.; Safgren, S. L.; *et al.* Targeted Delivery of Gemcitabine to Pancreatic Adenocarcinoma Using Cetuximab as a Targeting Agent. *Cancer Res.* **2008**, *68*, 1970–1978.
10. Papa, A.-L.; Basu, S.; Sengupta, P.; Banerjee, D.; Sengupta, S.; Harfouche, R. Mechanistic Studies of Gemcitabine-Loaded Nanoplatforms in Resistant Pancreatic Cancer Cells. *BMC Cancer* **2012**, *12*, 419.
11. Paolino, D.; Cosco, D.; Racanicchi, L.; Trapasso, E.; Celia, C.; Iannone, M.; Puxeddu, E.; Costante, G.; Filetti, S.; Russo, D.; *et al.* Gemcitabine-Loaded PEGylated Unilamellar Liposomes *vs* GEMZAR: Biodistribution, Pharmacokinetic Features and *In Vivo* Antitumor Activity. *J. Controlled Release* **2010**, *144*, 144–150.
12. Erkan, M. Understanding the Stroma of Pancreatic Cancer: Co-evolution of the Microenvironment with Epithelial Carcinogenesis. *J. Pathol.* **2013**, *231*, 4–7.
13. Baker, J. A. R.; Wickremsinhe, E. R.; Li, C. H.; Oluyedun, O. A.; Dantzig, A. H.; Hall, S. D.; Qian, Y.-w.; Ring, B. J.; Wrighton, S. A.; Guo, Y. Pharmacogenomics of Gemcitabine Metabolism: Functional Analysis of Genetic Variants in Cytidine Deaminase and Deoxycytidine Kinase. *Drug Metab. Dispos.* **2013**, *41*, 541–545.
14. Sugahara, K. N.; Teesalu, T.; Karmali, P. P.; Kotamraju, V. R.; Agemy, L.; Greenwald, D. R.; Ruoslahti, E. Coadministration of a Tumor-Penetrating Peptide Enhances the Efficacy of Cancer Drugs. *Science* **2010**, *328*, 1031–1035.
15. Goel, S.; Duda, D. G.; Xu, L.; Munn, L. L.; Boucher, Y.; Fukumura, D.; Jain, R. K. Normalization of the Vasculature for Treatment of Cancer and Other Diseases. *Physiol. Rev.* **2011**, *91*, 1071–1121.
16. Winkler, E. A.; Bell, R. D.; Zlokovic, B. V. Central Nervous System Pericytes in Health and Disease. *Nat. Neurosci.* **2011**, *14*, 1398–1405.
17. Darland, D. C.; D'Amore, P. A. TGF-β Is Required for the Formation of Capillary-like Structures in Three-Dimensional Cocultures of 10T1/2 and Endothelial Cells. *Angiogenesis* **2001**, *4*, 11–20.
18. Lammerts, E.; Roswall, P.; Sundberg, C.; Gotwals, P. J.; Koteliansky, V. E.; Reed, R. K.; Heldin, N.-E.; Rubin, K. Interference with TGF-β1 and -β3 in Tumor Stroma Lowers Tumor Interstitial Fluid Pressure Independently of Growth in Experimental Carcinoma. *Int. J. Cancer* **2002**, *102*, 453–462.
19. ten Dijke, P.; Arthur, H. M. Extracellular Control of TGF-β Signalling in Vascular Development and Disease. *Nat. Rev. Mol. Cell. Biol.* **2007**, *8*, 857–869.
20. Antonelli-Orlidge, A.; Saunders, K. B.; Smith, S. R.; D'Amore, P. A. An Activated Form of Transforming Growth Factor Beta Is Produced by Cocultures of Endothelial Cells and Pericytes. *Proc. Natl. Acad. Sci. U.S.A.* **1989**, *86*, 4544–4548.
21. Walshe, T. E.; Saint-Geniez, M.; Maharaj, A. S. R.; Sekiyama, E.; Maldonado, A. E.; D'Amore, P. A. TGF-beta Is Required for Vascular Barrier Function, Endothelial Survival and Homeostasis of the Adult Microvasculature. *PLoS One* **2009**, *4*, e5149.
22. Yingling, J. M.; Blanchard, K. L.; Sawyer, J. S. Development of TGF-β Signalling Inhibitors for Cancer Therapy. *Nat. Rev. Drug Discovery* **2004**, *3*, 1011–1022.
23. Vogt, J.; Traynor, R.; Sapkota, G. P. The Specificities of Small Molecule Inhibitors of the TGF-β and BMP Pathways. *Cell. Signalling* **2011**, *23*, 1831–1842.
24. Meng, H.; Xue, M.; Xia, T.; Ji, Z.; Tarn, D. Y.; Zink, J. I.; Nel, A. E. Use of Size and a Copolymer Design Feature To Improve the Biodistribution and the Enhanced Permeability and Retention Effect of Doxorubicin-Loaded Mesoporous Silica Nanoparticles in a Murine Xenograft Tumor Model. *ACS Nano* **2011**, *5*, 4131–4144.
25. Meng, H.; Mai, W. X.; Zhang, H.; Xue, M.; Xia, T.; Lin, S.; Wang, X.; Zhao, Y.; Ji, Z.; Zink, J. I.; *et al.* Codelivery of an Optimal Drug/siRNA Combination Using Mesoporous Silica Nanoparticles To Overcome Drug Resistance in Breast Cancer *in Vitro* and *in Vivo*. *ACS Nano* **2013**, *7*, 994–1005.
26. Estrella, V.; Chen, T.; Lloyd, M.; Wojtkowiak, J.; Cornnell, H. H.; Ibrahim-Hashim, A.; Bailey, K.; Balagurunathan, Y.; Rothberg, J. M.; Sloane, B. F.; *et al.* Acidity Generated by the Tumor Microenvironment Drives Local Invasion. *Cancer Res.* **2013**, *73*, 1524–1535.
27. Song, N.; Huang, Y.; Shi, H.; Yuan, S.; Ding, Y.; Song, X.; Fu, Y.; Luo, Y. Overexpression of Platelet-Derived Growth Factor-BB Increases Tumor Pericyte Content *via* Stromal-Derived Factor-1α/CXCR4 Axis. *Cancer Res.* **2009**, *69*, 6057–6064.

28. Bergers, G.; Song, S. The Role of Pericytes in Blood-Vessel Formation and Maintenance. *Neuro-Oncology* **2005**, *7*, 452–464.
29. Varelas, X.; Samavarchi-Tehrani, P.; Narimatsu, M.; Weiss, A.; Cockburn, K.; Larsen, B. G.; Rossant, J.; Wrana, J. L. The Crumbs Complex Couples Cell Density Sensing to Hippo-Dependent Control of the TGF-β-SMAD Pathway. *Dev. Cell.* **2010**, *19*, 831–844.
30. Chen, J.; Shearer, G. C.; Chen, Q.; Healy, C. L.; Beyer, A. J.; Nareddy, V. B.; Gerdes, A. M.; Harris, W. S.; O'Connell, T. D.; Wang, D. Omega-3 Fatty Acids Prevent Pressure Overload-Induced Cardiac Fibrosis through Activation of Cyclic GMP/Protein Kinase G Signaling in Cardiac Fibroblasts. *Circulation* **2011**, *123*, 584–593.
31. Farace, P.; Merigo, F.; Fiorini, S.; Nicolato, E.; Tambalo, S.; Daducci, A.; Degrassi, A.; Sbarbati, A.; Rubello, D.; Marzola, P. DCE-MRI Using Small-Molecular and Albumin-Binding Contrast Agents in Experimental Carcinomas with Different Stromal Content. *Eur. J. Radiol.* **2011**, *78*, 52–59.
32. Ferrari, M. Cancer Nanotechnology: Opportunities and Challenges. *Nat. Rev. Cancer* **2005**, *5*, 161–171.
33. Fakhrejahani, E.; Toi, M. Tumor Angiogenesis: Pericytes and Maturation Are Not To Be Ignored. *J. Oncol.* **2012**, Article ID 261750, DOI: 10.1155/2012/261750.
34. Oostendorp, M.; Douma, K.; Hackeng, T. M.; Dirksen, A.; Post, M. J.; van Zandvoort, M. A. M. J.; Backes, W. H. Quantitative Molecular Magnetic Resonance Imaging of Tumor Angiogenesis Using cNGR-Labeled Paramagnetic Quantum Dots. *Cancer Res.* **2008**, *68*, 7676–7683.
35. Mulder, W. J. M.; Strijkers, G. J.; Habets, J. W.; Bleeker, E. J. W.; van der Schaft, D. W. J.; Storm, G.; Koning, G. A.; Griffioen, A. W.; Nicolay, K. MR Molecular Imaging and Fluorescence Microscopy for Identification of Activated Tumor Endothelium Using a Bimodal Lipidic Nanoparticle. *FASEB J.* **2005**, *19*, 2008–2010.
36. Ranney, D.; Antich, P.; Dadey, E.; Mason, R.; Kulkarni, P.; Singh, O.; Chen, H.; Constantanescu, A.; Parkey, R. Dermatan Carriers for Neovascular Transport Targeting, Deep Tumor Penetration and Improved Therapy. *J. Controlled Release* **2005**, *109*, 222–235.
37. Agemy, L.; Sugahara, K. N.; Kotamraju, V. R.; Gujraty, K.; Girard, O. M.; Kono, Y.; Mattrey, R. F.; Park, J.-H.; Sailor, M. J.; Jimenez, A. I.; *et al.* Nanoparticle-Induced Vascular Blockade in Human Prostate Cancer. *Blood* **2010**, *116*, 2847–2856.
38. Straubinger, R. M.; Hong, K.; Friend, D. S.; Papahadjopoulos, D. Endocytosis of Liposomes and Intracellular Fate of Encapsulated Molecules: Encounter with a Low pH Compartment After Internalization in Coated Vesicles. *Cell* **1983**, *32*, 1069–1079.
39. Federico, C.; Morittu, V.; Britti, D.; Trapasso, E.; Cosco, D. Gemcitabine-Loaded Liposomes: Rationale, Potentialities and Future Perspectives. *Int. J. Nanomed.* **2012**, *2012*, 5423–5436.
40. Celano, M.; Calvagno, M.; Bulotta, S.; Paolino, D.; Arturi, F.; Rotiroti, D.; Filetti, S.; Fresta, M.; Russo, D. Cytotoxic Effects of Gemcitabine-Loaded Liposomes in Human Anaplastic Thyroid Carcinoma Cells. *BMC Cancer* **2004**, *4*, 63.
41. Haran, G.; Cohen, R.; Bar, L. K.; Barenholz, Y. Transmembrane Ammonium Sulfate Gradients in Liposomes Produce Efficient and Stable Entrapment of Amphipathic Weak Bases. *Biochim. Biophys. Acta* **1993**, *1151*, 201–215.
42. Castelli, F.; Raudino, A.; Fresta, M. A Mechanistic Study of the Permeation Kinetics through Biomembrane Models: Gemcitabine–Phospholipid Bilayer Interaction. *J. Colloid Interface Sci.* **2005**, *285*, 110–117.
43. Glezerman, I.; Kris, M.; Miller, V.; Seshan, S.; Flombaum, C. Gemcitabine Nephrotoxicity and Hemolytic Uremic Syndrome: Report of 29 Cases from a Single Institution. *Clin. Nephrol.* **2009**, *71*, 130–139.
44. Frese, K. K.; Neesse, A.; Cook, N.; Bapiro, T. E.; Lolkema, M. P.; Jodrell, D. I.; Tuveson, D. A. nab-Paclitaxel Potentiates Gemcitabine Activity by Reducing Cytidine Deaminase Levels in a Mouse Model of Pancreatic Cancer. *Cancer Discovery* **2012**, *2*, 260–269.
45. Liu, J.; Liao, S.; Diop-Frimpong, B.; Chen, W.; Goel, S.; Naxerova, K.; Ancukiewicz, M.; Boucher, Y.; Jain, R. K.; Xu, L. TGF-β Blockade Improves the Distribution and Efficacy of Therapeutics in Breast Carcinoma by Normalizing the Tumor Stroma. *Proc. Natl. Acad. Sci. U.S.A.* **2012**, *109*, 16618–16623.
46. Ji, T.; Zhao, Y.; Ding, Y.; Nie, G. Using Functional Nanomaterials To Target and Regulate the Tumor Microenvironment: Diagnostic and Therapeutic Applications. *Adv. Mater.* **2013**, *12*, 3508–3525.
47. Dreaden, E. C.; Mwakwari, S. C.; Austin, L. A.; Kieffer, M. J.; Oyelere, A. K.; El-Sayed, M. A. Small Molecule–Gold Nanorod Conjugates Selectively Target and Induce Macrophage Cytotoxicity towards Breast Cancer Cells. *Small* **2012**, *8*, 2819–2822.
48. Jacobetz, M. A.; Chan, D. S.; Neesse, A.; Bapiro, T. E.; Cook, N.; Frese, K. K.; Feig, C.; Nakagawa, T.; Caldwell, M. E.; Zecchini, H. I.; *et al.* Hyaluronan Impairs Vascular Function and Drug Delivery in a Mouse Model of Pancreatic Cancer. *Gut* **2013**, *62*, 112–120.
49. Provenzano, P. P.; Cuevas, C.; Chang, A. E.; Goel, V. K.; Von Hoff, D. D.; Hingorani, S. R. Enzymatic Targeting of the Stroma Ablates Physical Barriers to Treatment of Pancreatic Ductal Adenocarcinoma. *Cancer Cell* **2012**, *21*, 418–429.
50. Kultti, A.; Li, X.; Jiang, P.; Thompson, C. B.; Frost, G. I.; Shepard, H. M. Therapeutic Targeting of Hyaluronan in the Tumor Stroma. *Cancers* **2012**, *4*, 873–903.
51. ABRAXANE Plus Gemcitabine Demonstrates Significant Survival Advantage in Phase III Study of Patients with Advanced Pancreatic Cancer, http://ir.celgene.com/phoenix.zhtml?c=111960&p=irol-newsArticle&ID=1776848-&highlight=.
52. Von Hoff, D. D.; Ramanathan, R. K.; Borad, M. J.; Laheru, D. A.; Smith, L. S.; Wood, T. E.; Korn, R. L.; Desai, N.; Trieu, V.; Iglesias, J. L.; *et al.* Gemcitabine Plus nab-Paclitaxel Is an Active Regimen in Patients with Advanced Pancreatic Cancer: A Phase I/II Trial. *J. Clin. Oncol.* **2011**, *29*, 4548–4554.
53. Kano, M. R.; Komuta, Y.; Iwata, C.; Oka, M.; Shirai, Y.-t.; Morishita, Y.; Ouchi, Y.; Kataoka, K.; Miyazono, K. Comparison of the Effects of the Kinase Inhibitors Imatinib, Sorafenib, and Transforming Growth Factor-β Receptor Inhibitor on Extravasation of Nanoparticles from Neovasculature. *Cancer Sci.* **2009**, *100*, 173–180.
54. Quatromoni, J.; Wang, Y.; Vo, D.; Morris, L.; Jazirehi, A.; McBride, W.; Chatila, T.; Koya, R.; Economou, J. T Cell Receptor (TCR)-Transgenic CD8 Lymphocytes Rendered Insensitive to Transforming Growth Factor Beta (TGF-Beta) Signaling Mediate Superior Tumor Regression in an Animal Model of Adoptive Cell Therapy. *J. Transl. Med.* **2012**, *10*, 127.
55. Zhang, Q.; Yang, X.; Pins, M.; Javonovic, B.; Kuzel, T.; Kim, S.-J.; Parijs, L. V.; Greenberg, N. M.; Liu, V.; Guo, Y.; *et al.* Adoptive Transfer of Tumor-Reactive Transforming Growth Factor-Beta Insensitive $CD8^+$ T Cells: Eradication of Autologous Mouse Prostate Cancer. *Cancer Res.* **2005**, *65*, 1761–1769.
56. Wojtkowiak, J. W.; Rothberg, J. M.; Kumar, V.; Schramm, K. J.; Haller, E.; Proemsey, J. B.; Lloyd, M. C.; Sloane, B. F.; Gillies, R. J. Chronic Autophagy Is a Cellular Adaptation to Tumor Acidic pH Microenvironments. *Cancer Res.* **2012**, *72*, 3938–3947.
57. Jahde, E.; Volk, T.; Atema, A.; Smets, L. A.; Glusenkamp, K.-H.; Rajewsky, M. F. pH in Human Tumor Xenografts and Transplanted Rat Tumors: Effect of Insulin, Inorganic Phosphate, and m-Iodobenzylguanidine. *Cancer Res.* **1992**, *52*, 6209–6215.
58. Guillaumond, F.; Leca, J.; Olivares, O.; Lavaut, M.-N.; Vidal, N.; Berthezne, P.; Dusetti, N. J.; Loncle, C.; Calvo, E.; Turrini, O.; *et al.* Strengthened Glycolysis under Hypoxia Supports Tumor Symbiosis and Hexosamine Biosynthesis in Pancreatic Adenocarcinoma. *Proc. Natl. Acad. Sci. U.S.A.* **2013**, *110*, 3919–3924.
59. Swietach, P.; Vaughan-Jones, R.; Harris, A. Regulation of Tumor pH and the Role of Carbonic Anhydrase. *Cancer Metastasis Rev.* **2007**, *26*, 299–310.

60. Liu, S.; Redeye, V.; Kuremsky, J. G.; Kuhnen, M.; Molinolo, A.; Bugge, T. H.; Leppla, S. H. Intermolecular Complementation Achieves High-Specificity Tumor Targeting by Anthrax Toxin. *Nat. Biotechnol.* **2005**, *23*, 725–730.
61. Meng, H.; Xing, G.; Sun, B.; Zhao, F.; Lei, H.; Li, W.; Song, Y.; Chen, Z.; Yuan, H.; Wang, X.; *et al.* Potent Angiogenesis Inhibition by the Particulate Form of Fullerene Derivatives. *ACS Nano* **2010**, *4*, 2773–2783.
62. Hartley, J. A.; Spanswick, V. J.; Brooks, N.; Clingen, P. H.; McHugh, P. J.; Hochhauser, D.; Pedley, R. B.; Kelland, L. R.; Alley, M. C.; Schultz, R.; *et al.* SJG-136 (NSC 694501), a Novel Rationally Designed DNA Minor Groove Interstrand Cross-Linking Agent with Potent and Broad Spectrum Antitumor Activity: Part 1: Cellular Pharmacology, *In Vitro* and Initial *In Vivo* Antitumor Activity. *Cancer Res.* **2004**, *64*, 6693–6699.
63. Kubota, T.; Matsuzaki, S. W.; Hoshiya, Y.; Watanabe, M.; Kitajima, M.; Asanuma, F.; Yamada, Y.; Koh, J.-I. Antitumor Activity of Paclitaxel Against Human Breast Carcinoma Xenografts Serially Transplanted into Nude Mice. *J. Surg. Oncol.* **1997**, *64*, 115–121.
64. Kano, M. R.; Bae, Y.; Iwata, C.; Morishita, Y.; Yashiro, M.; Oka, M.; Fujii, T.; Komuro, A.; Kiyono, K.; Kaminishi, M.; *et al.* Improvement of Cancer-Targeting Therapy, Using Nanocarriers for Intractable Solid Tumors by Inhibition of TGF-β Signaling. *Proc. Natl. Acad. Sci. U.S.A.* **2007**, *104*, 3460–3465.
65. Feng, X.-H.; Derynck, R. Specificity and Versatility in TGF-β Signaling through Smads. *Annu. Rev. Cell. Dev. Biol.* **2005**, *21*, 659–693.